공학석사 학위논문

Far-field Analysis of Ground Heaving and Fault Reactivation for the Reference and the Alternative Disposal Systems of High-Level Radioactive Waste

고준위방사성폐기물의 기준 및 대안 처분시스템에서의 지표면 융기와 단층 재활성화 원계 해석

2022 년 8 월

서울대학교 대학원
에너지시스템공학부
서은진

Far-field Analysis of Ground Heaving and Fault Reactivation for the Reference and the Alternative Disposal Systems of High-Level Radioactive Waste

지도교수 민기복

이 논문을 공학석사 학위논문으로 제출함

2022 년 8 월

서울대학교 대학원
에너지시스템공학부

서 은 진

서은진의 공학석사 학위논문을 인준함
2022 년 8 월

Chair	전석원	(Seal)
Vice Chair	민기복	(Seal)
Examiner	송재준	(Seal)

Abstract

Far-field Analysis of Ground Heaving and Fault Reactivation for the Reference and the Alternative Disposal Systems of High-Level Radioactive Waste

Eunjin Seo

The Graduate School

Department of Energy Systems Engineering

Rock Mechanics and Rock Engineering Laboratory

Seoul National University

The decay heat and change in the corresponding thermal stress of high-level radioactive waste (HLW) disposal systems affect the local stress condition and this can induce fault reactivation around the system. Although studies on the effect of earthquake on disposal systems have been performed with a focus on the canister integrity, the possibility of inducing fault reactivation due to geological repository has not received enough attention.

In this study, numerical models were developed for the coupled thermo–hydro–mechanical (THM) processes of the rock mass around a

reference disposal system and alternative disposal systems, including double-canister, double-layered, and triple-layered disposal systems. The analysis of the coupled THM behavior revealed that compressive stress inside the disposal system and tensile stress at the ground surface were generated in all the disposal systems. In addition, the maximum ground heaving in the multi-layered disposal systems was larger than that of the reference disposal system by approximately 10 cm. Not only the maximum value, but also the heaving angle and velocity were found to be large in the double-layered alternative disposal system.

Based on the numerical results, the fault reactivation around the disposal systems was firstly investigated by evaluating the change in the Coulomb failure stress (CFS) at a given fault orientation (90/30). An increase in the CFS was mainly observed in three regions: in the middle of the disposal system, at the ground surface above the disposal system, and in the vicinity of the boundary. In addition, compared to other models, the triple-layered disposal system exhibited the most significant increase in the CFS at 700 m disposal depth. The change in the CFS at all the dip and dip direction of faults was also analyzed using stereonet. The change in the CFS was significantly affected by the dip of faults in the middle of the disposal system, and the dip and dip direction of faults in the vicinity of the disposal system depending on the direction of the principal thermal stress changes. In the case of the alternative disposal systems, even at a distance of approximately 3 km from the boundary, the CFS could increase in several direction of the faults at the disposal depth after a very long time.

Consequently, although the disposal area can be reduced in the alternative disposal systems, the possibility of fault reactivation and the ground heaving are higher than in the reference disposal system. Additionally, as the fault reactivation depends on the initial stress and the friction coefficient of the fault, it is important to obtain the accurate information related to this before a geological repository operation.

Keyword: Geological repository of high-level radioactive waste, alternative disposal system, thermo-hydro-mechanical modeling, coulomb failure stress, fault reactivation

Student Number: 2020-28963

TABLE OF CONTENTs

List of Tables

List of Figures

보존용 학위논문 정오표

페이지	정정 전	정정 후
p. 20 : 14 p. 23 : 5 p. 44 : 6 p. 52 : 11	Cho et al. (2020) Table 3.2. layers heat	Lee et al. (2020b) Table 3.2 layers. heat.

Chapter 1. Introduction

1.1 Background

Currently, there is a total of 24 operating nuclear power plants in Korea, and approximately 30% of the total power generation in the nation is dependent on nuclear power generation (IAEA, 2020). The spent nuclear fuels are classified as high-level radioactive Wastes (HLW) and are currently managed in wet or dry storage (Lee et al., 2020b). However, they should be isolated for a very long time because of their radioactivity. Particularly, Lee et al. (2020b) reported that more than 60,000 assemblies of pressurized light water reactor (PWR) fuel type should be disposed by 2080 (Figure 1.1).

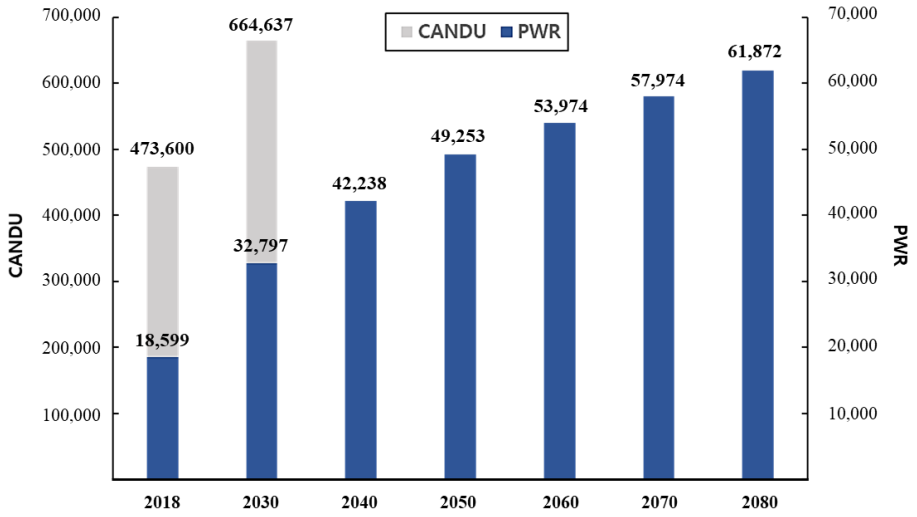

Figure 1.1 Spent nuclear fuel arising from domestic nuclear power plants (modified from Lee et al., 2020b)

Regarding the final disposal of nuclear waste, deep geological disposal system is considered as one of the most promising concepts in many countries. The domestic 「Basic Plan for High Level Waste Management」 established in Korea (APEC, 2016) is also based on the deep disposal concept (e.g., KBS-3), which is adopted in Sweden and Finland. In the disposal system, the maximum temperature at the interface between canister and buffer should not exceed 100 ℃. If the temperature exceeds this limit, the phase change of bentonite in buffer will occur, which will result in the instability of the engineered barrier system around the nuclear waste.

In Korea, the Korean reference disposal System (KRS) was first developed in 2007 (Lee et al., 2007). Subsequently, KRS-HB, which reflects the characteristics of high burn-up spent nuclear fuel generated by domestic nuclear power plants, was developed in 2013 (Kim et al., 2013). Lastly, by considering the characteristics of PWR type and pressurized heavy water reactor type (PHWR, CANDU) spent nuclear fuel in Korea, KRS^{+} was developed (Lee et al., 2020b), and the coupled thermo–hydro–mechanical (THM) analysis of this system has been conducted (Kim et al., 2021).

1.2 Previous studies

It is essential to minimize the disposal area, and this should be considered important not only in terms of communication with residents but also in terms of high population density for countries, such as Korea. Therefore, various alternative disposal concepts, such as multi-layered and multi-canister disposal concepts have been proposed to reduce the disposal area compared to that required by the reference disposal system (Figure 1.2).

Lee et al. (2017) conducted a thermal analysis for multi-layered and multi-canister disposal concepts, and found that the multi-canister disposal concept could not satisfy the required thermal condition, even if the deposition hole spacing is twice as large as that of KRS-HB. However, as the fuel type considered in the study of Lee et al. (2017) was based on KRS, the result may differ from that of KRS^{+}. In addition, Lee et al. (2020a) conducted a coupled THM analysis for double- and triple-layered disposal concepts based on KRS, and analyzed the thermal, hydraulic, and mechanical behavior near the disposed nuclear waste, including canister, buffer, and backfill. The results revealed that the ideal spacing between layers in the triple-layered disposal concepts should be 200 m and the deposition hole spacing should be 8 m.

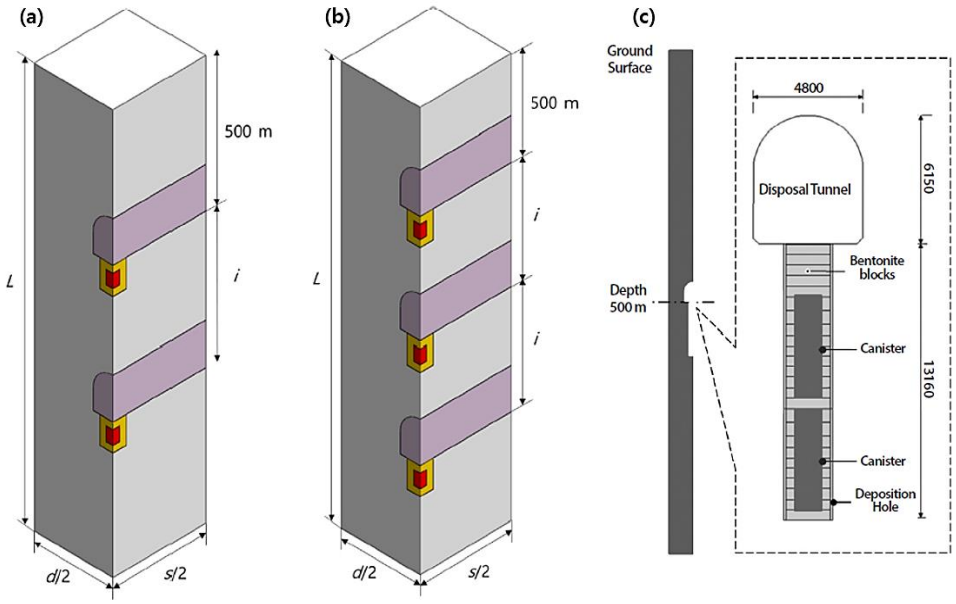

Figure 1.2 Geometry of the alternative disposal systems; (a) Double-layer concept (b) Triple-layer concept (c) Double-canister concept (Lee et al., 2020a; Lee et al., 2017)

Attempts have been made to analyze the thermal stress around the geological repository in a far-field scale. For example, Min et al. (2013) conducted a thermo-mechanical analysis for the geological repository in Sweden using a three-dimensional (3D) far-field numerical model, and mainly investigated the thermal stress evolutions and the shear slip zone. The far-field model used in the study was the basic geometry referenced in the numerical analysis of this research.

Additionally, Urpi et al. (2019) investigated the fault reactivation around the geological repository of HLW in the clay formation. The clay formation was considered as a bedrock and the fault with an 80° dip was assumed near

the geological repository. In addition, thermal pressurization was observed, in which the pore pressure increased with heating, and fault slip evolution was investigated based on numerical THM results.

1.3 Motivation and objectives

The aforementioned THM studies only focused on the near-field scale based on the tunnel spacing and the deposition hole spacing domain. Although Min et al. (2013) attempted to analyze thermal stress in a far-field scale, they only conducted thermo-mechanical analysis for the Forsmark site and the domain size was not sufficiently large to remove the boundary effect on the temperature distribution.

Studies on the fault reactivation in and around geological repository are still at an embryonic stage, and more systematic studies are necessary. Furthermore, the possibility of fault reactivation in alternative disposal systems needs to be investigated. In addition, the evolution of thermal stress, pore pressure, and the other coupled results should be investigated based on coupled THM numerical results as these can affect the fault reactivation around a geological repository. In addition, it is essential to evaluate the safety of disposal systems based on the coupled THM behavior, particularly, that of high-level waste disposal systems. Owing to the importance of evaluating the stability in consideration of numerous scenarios, such as earthquakes and ice

ages, as important rock mechanical factors, it is important to analyze the induced or triggered fault slip around the geological repository for the safety and performance assessment of the geological repository.

The main objective of this research was to assess the possibility of fault reactivation around disposal systems. To evaluate the fault reactivation, first, numerical models were constructed based on the finite element method (FEM) to predict the coupled THM behavior of the rock mass around the geological repository of HLW including the ground heaving at the ground surface. In addition, far-field numerical models in a few km scales were constructed. To analyze not only the reference model consisting of a single deposition hole but also the possibility of fault reactivation at a long distance about few kilometers, a quarter model that considered the entire disposal system as a thin rectangular plate was constructed.

Based on the constructed numerical models, the Coulomb failure stress (CFS), which is a good indicator to demonstrate the possibility of the fault reactivation, was used. After verifying the numerical results of the THM behaviors in the far-field model, the possibility of fault reactivation was investigated. For a preliminary analysis of the risk of fault reactivation according to the distance from the disposal system, the possibility of reactivation of the fault around the disposal system was evaluated by analyzing the CFS change, which reflects the possibility of the fault reactivation with given stress changes.

Chapter 2. Background and theory

2.1 Coupled thermo-hydro-mechanical processes

Around the disposal system the host rock mass is heated up and thermal expansion will occur due to decay heat from the nuclear waste. Thermal strain induces the thermal stress around the geological repository, and this result in perturbation of local stress state. Therefore, the coupled thermo-hydro-mechanical (THM) behavior is important around the geological repository. This coupled THM process is summarized as a diagram shown in Figure 2.1.

In this section, the governing equations for the coupled THM process is introduced. In elaboration of the mathematical equations, it is assumed that the rock mass is isotropic, the rock mass is fully water saturated porous medium, and the water phase variation is not considered. To explain the coupling in the porous medium, energy conservation, mass conservation and equation of stresses are used.

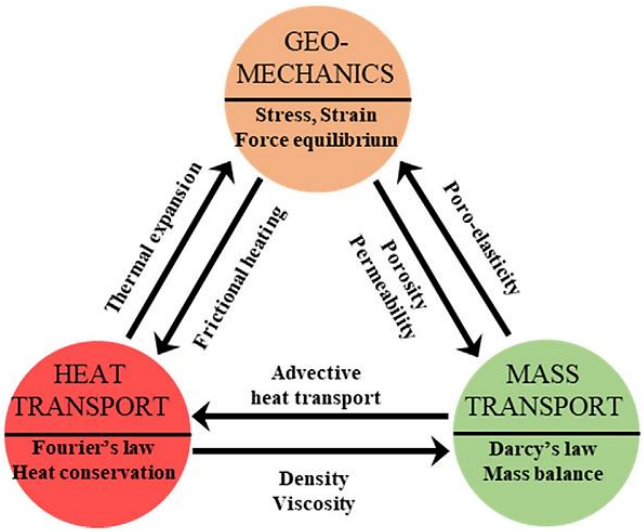

Figure 2.1 A schematic diagram of the coupled thermo-hydro-mechanical process in the reservoir. (Guo et al., 2020)

The equation of stresses can be explained as a function of strain, fluid pressure and thermal stress in accordance with the linear theory of poro-thermoelasticity as the following equation (McTigue, 1986).

$$\Delta\boldsymbol{\sigma} = 2G\left[\boldsymbol{\varepsilon} + \frac{\nu}{1-2\nu}\varepsilon_v \boldsymbol{I}\right] - \alpha_B \Delta p \boldsymbol{I} - 3K\alpha_T \Delta T \boldsymbol{I} \qquad (2.1)$$

where $\Delta\boldsymbol{\sigma}$ is total stress tensor, $\boldsymbol{\varepsilon}$ is the strain tensor related to the solid displacements $\mathbf{u}$ with an equation of $\boldsymbol{\varepsilon} = [(\nabla\mathbf{u} + \nabla\mathbf{u})^{\mathrm{t}}]/2$, $\boldsymbol{I}$ is the identify matrix, G and ν are the shear modulus and the Poisson's ratio, α_B is the Biot coefficient and K is the bulk modulus of the rock.

The last term in the right side of the Eq. (2.1) shows the thermally induced stress. This thermal stress is basically caused by the thermal expansion of the rock when it is heated up. Here, in order to consider the volumetric thermal strain, volumetric thermal strain obtained by multiplying three times to the linear thermal expansion coefficient. And difference from the reference temperature and the Elastic modulus are multiplied to calculate the thermal stress. If the rock is heated while free to expand, the thermal stresses are not induced. However, in the subsurface, rocks are usually constrained to one extent or another, so the thermal stresses will be roughly in the order of $3K\alpha_T\Delta T$ (Jeager et al., 2009).

In the porous media, since the fluid flow follows the Darcy's law, the fluid velocity is expressed as a function of the pressure gradient, the fluid viscosity, and the permeability of the porous medium as described in the following.

$$\boldsymbol{q} = -\frac{k}{\mu}(\nabla p + \rho g \nabla z) \tag{2.2}$$

where k is the permeability, μ and ρ are the viscosity and density of fluid, respectively, which is also dependent on the pressure and temperature, g is the gravitational acceleration, and z is the vertical coordinate.

Considering the thermal expansion and the deformation of the porous matrix, the mass conservation of the fluid is formulated by the following equation (Ghassemi and Zheng, 2004).

$$\rho\alpha_B \frac{\partial \varepsilon_v}{\partial t} - (\phi\alpha_l + (1-\phi)\alpha_s)\frac{\partial T}{\partial t} + \rho\left(\frac{\phi}{K_l} + \frac{1-\phi}{K_s}\right)\frac{\partial p}{\partial t} = \nabla \cdot \left(\frac{\mathrm{k}}{\mu}\nabla p\right) + Q_m \tag{2.3}$$

where ε_v is volumetric strain, ϕ is the porosity of the rock mass, α_s and α_l are thermal expansion coefficients of solid and fluid, K_s and K_l are bulk modulus of solid and fluid, and Q_m is a mass source. The first term in left equation indicates the mechanical coupling in mass flow and the second term indicates temperature coupling in hydraulic behavior depending on thermal expansion coefficient.

Due to the difference in the thermal expansion coefficient of solid and fluid, it would affect the pore pressure changes during an increase of temperature, and it is called as thermal pressurization (Urpi et al., 2019). When the temperature increases, the pore space will be decreased due to thermal expansion. Since the fluid in pore pressure has a larger thermal expansion coefficient than the porous matrix, the fluid will be more expanded. This is the main mechanism of the thermal pressurization observed in bed rock which has low permeability and porosity.

Energy conservation equation is formulated by the following equation (McTigue, 1986):

$$\left(\rho_s C_s(1-\phi)+\rho_f C_f \phi\right)\frac{\partial T}{\partial t}+\rho C_f \boldsymbol{u}\cdot\nabla \mathrm{T} = \nabla\cdot\left((1-\phi)k_s+\phi k_f\right)\nabla T+Q \tag{2.4}$$

where C_s and C_f are the specific heat capacity of solid and fluid, Q is an external or internal heat source, $\boldsymbol{u}$ is the fluid velocity, and k_s and k_f are thermal conductivity of solid and fluid. The second term in left equation shows convection in fluid heat transfer and the right term of the Eq (2.4) shows conduction in the porous media.

In this research to conduct a fully coupled thermo-hydro-mechanical modeling, the hydraulic properties are considered to be changed by different temperature and pressure. Porosity and permeability are dependent on volumetric strain as shown the below equations to reflect the effect of the poro-elasticity and thermo-elasticity (Mainguy and Longuemare, 2002; Li et al., 2004; Tortike and Ali, 1993).

$$\phi = \phi_0 + \alpha_B \Delta\varepsilon_v + c_s(\alpha_B - \phi_0)\Delta p \tag{2.5}$$

$$\mathrm{k} = \mathrm{k}_0 \exp\left(\frac{5}{\phi}\varepsilon_v\right) \tag{2.6}$$

2.2 CFS (Coulomb Failure Stress) theory

The changes in temperature and pore pressure due to decay around the geological repository results in perturbation of local stress state, even at the distance, due to the coupled THM response of the porous rock matrix. The influence of this stress perturbation on the fault reactivation near the geological repository can be calculated in terms of change in Coulomb Failure Stress (CFS).

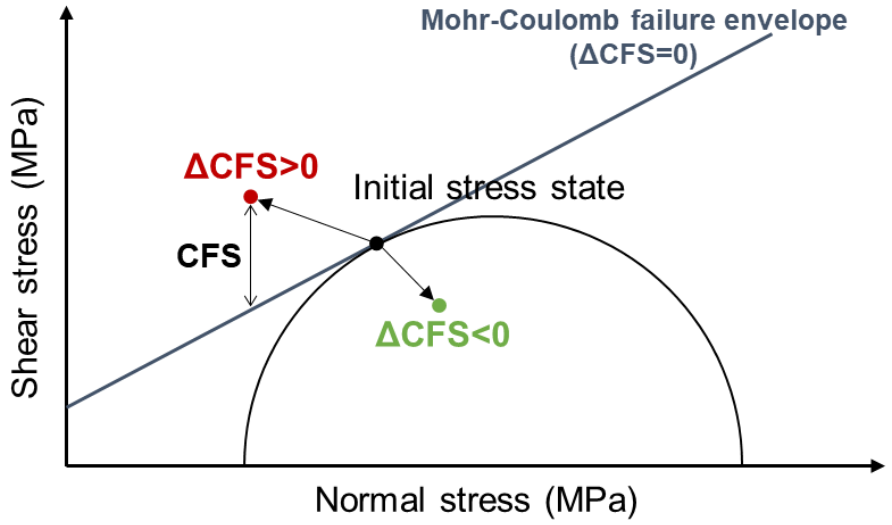

Figure 2.2. Schematic diagram of the Coulomb failure stress change with the Mohr-Coulomb failure criteria. Conceptually the initial stress represents the critically stressed state of the fault. The negative CFS change means fault stabilization and the positive CFS change means fault reactivation.

CFS is an efficient parameter to quantify the mechanical stability of a fault (Chang et al., 2018). The CFS physically means the difference between the Mohr-Coulomb failure criterion and the stress state of fault plane. If the Mohr-Coulomb failure criterion contacts to the Mohr circle, shear failure on that fault plane will occur. Thus, the CFS shows how far the stress state of the fault is from the specified Mohr-coulomb failure criterion and it means how much the fault is stable. Based on CFS theory, the possibility of the fault reactivation can be analyzed with the normal stress, shear stress, and pore pressure on the fault plane.

When analyzing the fault reactivation based on the CFS function, generally, the change of CFS is calculated due to the lack of original or initial stress state knowledge (Harris, 2000). The change of CFS is calculated as (Harris, 2000):

$$\Delta CFS = |\Delta\tau| + \mu(\Delta\sigma + \alpha\Delta P) \tag{2.7}$$

where μ is the friction coefficient of a fault, τ is the shear stress, σ is the normal stress, α is the Biot coefficient and P is the pore pressure. The positive sign of the normal stress change signifies an increase of tensile normal stress.

If a fault is under the critical state for shear failure, the positive change of CFS indicates fault reactivation, whereas the fault is stabilized in case of negative change of CFS (Figure 2.2). In the CFS theory, the initial stress, conceptually, represents the critically stressed state of the fault. Thus, the

reactivation of the faults could be different depending on the initial state of the fault. However, Zoback and Gorelick (2012) argue that most of the pre-existing faults in the crust in continental interiors are almost critically stressed based on the seismic catalogs recorded in central and eastern United States, southeastern Canada and south and east Asia. The increase of shear slip, tensile normal stress, and pore pressure makes the fault more unstable to shear slip. According to Stein (1999) and Reasenberg and Simpson (1992), a very small increase of the CFS, about 0.01 MPa, can trigger the earthquake when the fault is under critically stressed state.

Figure 2.3 shows the normal stress and the shear stress acting on a given arbitrary plane. When a stress field is defined by a stress tensor, three dimensional normal and shear stresses applied to the inclined fault plane can be calculated based on the Cauchy's law (Jeager et al., 2009).

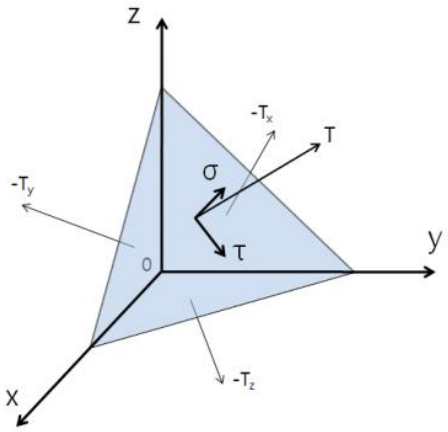

Figure 2.3 Normal and shear stresses acting on an arbitrary plane through a point (Lee, 2014)

A unit normal vector of the plane is given as

$$\boldsymbol{n}i = \begin{bmatrix} n_1 \\ n_2 \\ n_3 \end{bmatrix} \tag{2.8}$$

The three-dimensional stress tensor consists of nine components σ_{ij} that completely define the state of stress at a point inside a material in the deformed state:

$$\boldsymbol{\sigma}_{ij} = \begin{bmatrix} \sigma_{11} & \sigma_{12} & \sigma_{13} \\ \sigma_{21} & \sigma_{22} & \sigma_{23} \\ \sigma_{31} & \sigma_{32} & \sigma_{33} \end{bmatrix} \tag{2.9}$$

The traction vector, T is expressed with the stress tensor and the normal vector of the fault plane as following equation.

$$\boldsymbol{T}i = \begin{bmatrix} T_1 \\ T_2 \\ T_3 \end{bmatrix} = \boldsymbol{\sigma}_{\mathrm{ij}} n_j \tag{2.10}$$

The magnitude of the normal stress (σ) and shear stress (τ) of any stress vector $\boldsymbol{T}$ acting on an arbitrary plane with normal vector **n** at a given point is expressed as follows:

$$\sigma = \mathbf{T} \cdot \mathbf{n} \tag{2.11}$$

$$\tau = \sqrt{\mathbf{T^2} - \sigma^2} \tag{2.12}$$

Chapter 3. Numerical model

In this research, COMSOL Multiphysics 5.6, which is based on FEM, was used for the coupled thermo-hydro-mechanical modeling (COMSOL, 2004). COMSOL is well-developed with powerful interfaces, such as poroelasticity, thermal expansion, and heat transfer in porous media. Furthermore, COMSOL Multiphysics is a flexible partial differential equation solver. In addition, fully coupled governing equations for the THM behavior around the geological repository was simultaneously solved using COMSOL Multiphysics. To conduct fully coupled THM simulation, Darcy's law, Solid mechanics, and Heat transfer in porous media modules were employed.

3.1 Verification of numerical simulator

The coupled THM verification for COMSOL Multiphysics was carried out by Guo et al. (2020). In the numerical verification, the variation of temperature, pressure, and stress near the circular wellbore after sudden cooling (Figure 3.1) was analyzed by COMSOL Multiphysics. The initial temperature and pressure of the reservoir are 200 ℃ and 0 MPa, respectively. The hole radius is 0.1 m and the outer boundary of the wellbore was fixed. The wellbore was suddenly cooled down by water and maintained at 80 ℃. In this

numerical verification, the fully-saturated Granite was assumed and only thermally induced change in stresses and pore pressure are studied. It means that the far field pore pressure and stresses are considered to be zero.

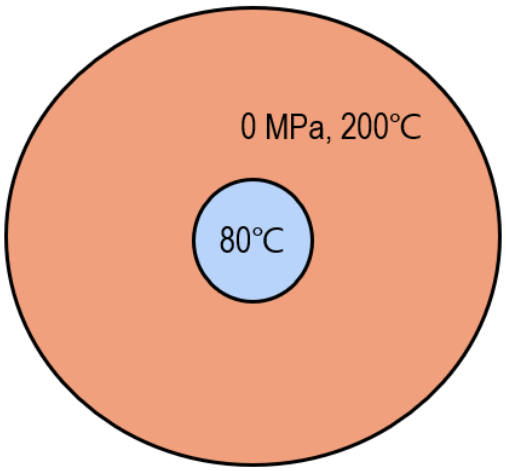

Figure 3.1 Geometric model and its initial and boundary conditions of THM coupling model verification (modified after Guo et al., 2020)

The thermo-hydro-mechanical properties used in the verification is shown in Table 3.1. And Guo et al. compared the analytical results from Ghassemi and Zhang (2004) to numerical results from COMSOL (Figure 3.2).

Table 3.1 Input parameters used in thermo-hydro-mechanical verification of COMSOL (Ghassemi and Zhang, 2004)

Parameter	value	Unit
Young's modulus E	37.5	GPa
Poisson's ratio ν	0.25	-
Biot coefficient α	0.41	-
Thermal conductivity λ	10.38	W/m/K
Specific heat capacityC	790	J/kg/K
Bulk modulus of fluid K_f	2.5	GPa
Fluid viscosity μ	3.55×10^{-4}	Pa·s
Porosity ϕ	0.01	-
Permeability k	4.053×10^{-19}	m^2

The numerical results and the analytical results are matched well in radial and tangential stresses, pore pressure variation and temperature variation depending on different time. In THM coupling, the temperature reduction causes the variation of fluid flow and stress field. After sudden cooling effect,

the pore pressure decreased up to 2 MPa, and the temperature decrease causes the tensile stress near the wellbore. The maximum tensile radial stress reaches 17.5 MPa and the tangential stress is up to 48.1 MPa. Although the stress influence is near the wellbore due to the slower temperature propagation, the generated large thermal stress causes the damage near the wellbore.

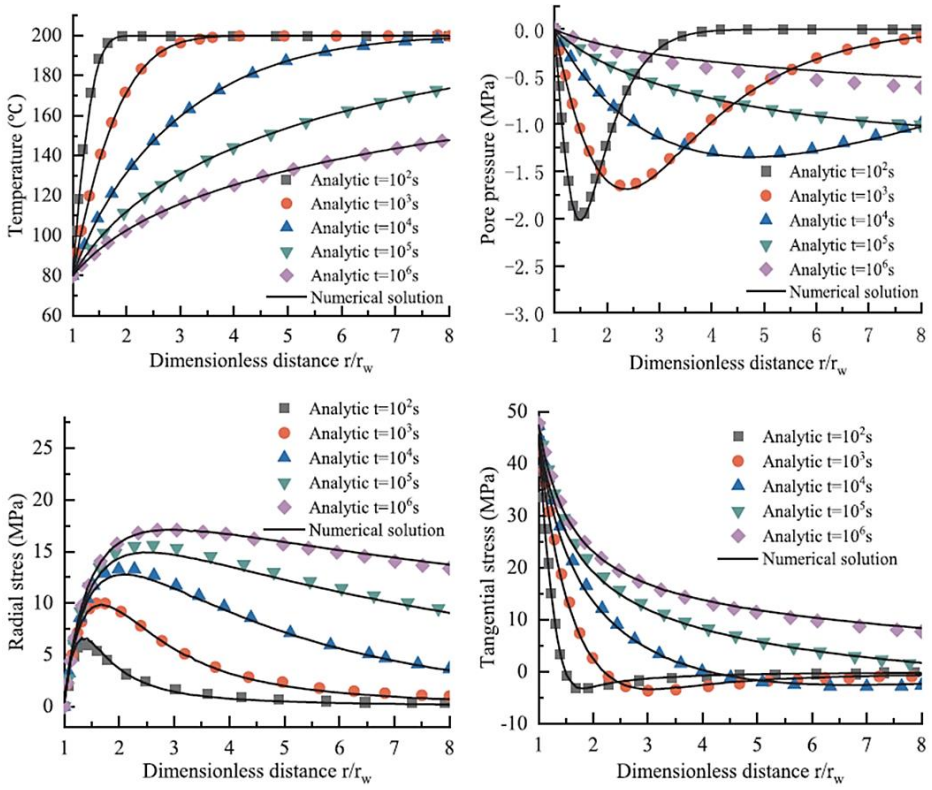

Figure 3.2 Coupled THM verification results over dimensionless distance at various time (Guo et al., 2020)

3.2 Numerical model description

3.2.1 Reference disposal system

In this study, the 3D numerical models were constructed as near-field and far-field models, as shown in Figure 3.3. The concept of thermoshearing in a far-field model was proposed by Min et al. (2013). The thermal behavior of the near-field and far-field models is compared in this section to demonstrate the validity of the far-field numerical model.

To prevent the boundary effect on the temperature, pore pressure, and stress fields at the repository level, the depth of the numerical model was set to 4,000 m. The near-field model consisted of one canister with a tunnel spacing of 40 m and a canister spacing of 7.5 m according to the KRS^{+} disposal concept (Lee et al., 2020a).

In the far-field model, however, the deposition hole, canister, and tunnels were lumped together as a thin rectangular plate with a uniform thickness. A quarter of the entire disposal system was considered as a symmetric model with a 5 km × 5 km × 4 km domain. According to Cho et al. (2020), the total number of the assemblies from a PWR fuel type that should be disposed in Korea in the 2080s is approximately 60,000. As one canister consists of four assemblies, this indicates that approximately 15,000 canisters should be disposed. Thus, in this research, it was assumed that 3,750 canisters will be

disposed in a symmetric quarter model to dispose the entire assemblies in 2080s.

When the shape of the disposal system was determined, the equivalent area suggested by Min et al. (2013) was not employed. This is because it was assumed that this will create difficulties in achieving an ideal square shape when constructing the actual disposal system in consideration of the tunnel and deposition hole spacings. Thus, the x-direction length was divided by the deposition hole spacing and the y-direction length by the tunnel spacing. In addition, to minimize the anisotropy of thermal stress according to the shape of the disposal system, the length of the x-direction and y-direction of the disposal system were adjusted to be almost the same. Here, it was assumed that there are 150 deposition holes along the x-direction and 25 tunnels along the y-direction in the 1,125 m x 1,000 m x 14 m disposal system.

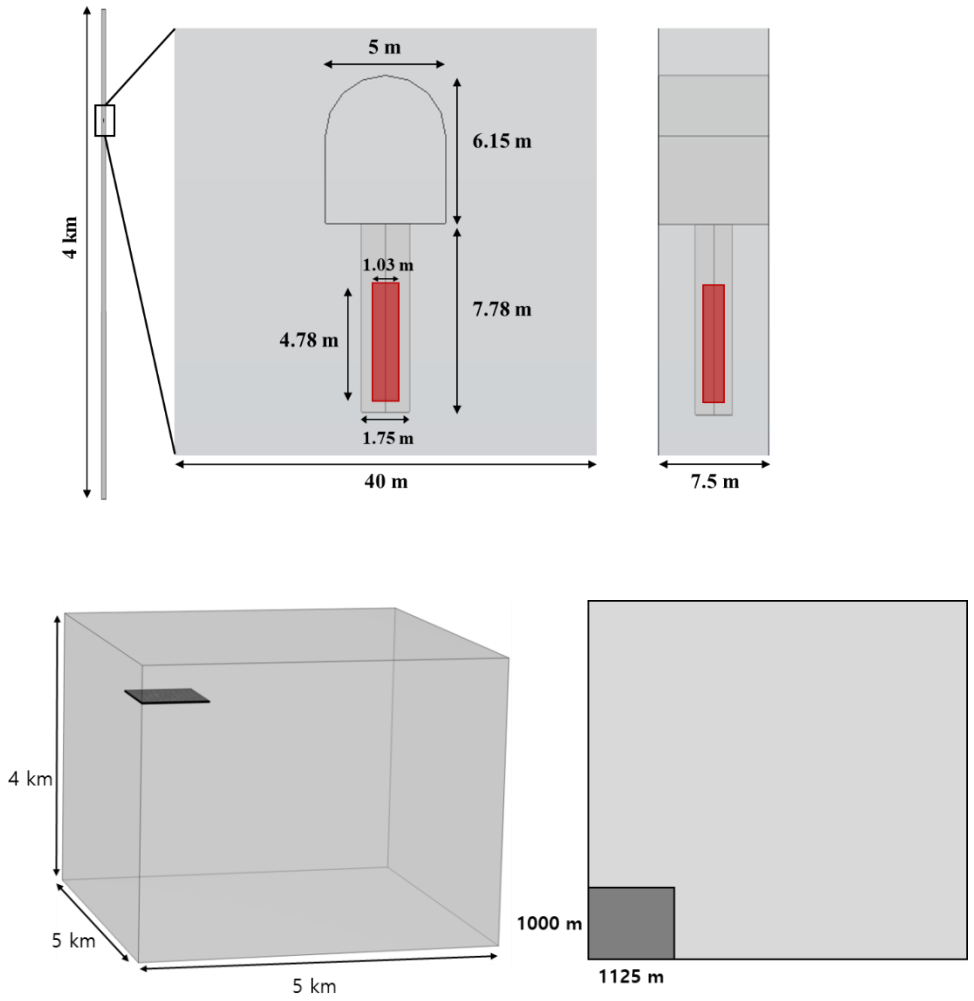

Figure 3.3 Geometry of the three-dimensional numerical model for the reference disposal system used in this study (top) near-field model (bottom) far-field model

To validate the efficacy of the far-field model compared to that of the near-field model, the thermal behavior of each numerical model was analyzed. In this research, the nuclear waste type is based on PWR. The decay heat from 1 tU in a PWR R-SNF fuel was expressed as follows (Eq. (3.1)) and each parameter in the equation is shown in Table 3.2. (Kim et al., 2021).

$$Q = y_0 + A_1 \times \exp\left(-\frac{t - x_0}{t_1}\right) + A_2 \times \exp\left(-\frac{(t - x_0)}{t_2}\right) + A_3 \times \exp\left(-\frac{t - x_0}{t_3}\right) \quad (3.1)$$

After considering that approximately 1.72 ton of Uranium will be stored in a KRS+ type canister, and this canister will be stored for 40 years in spent fuel pool to consider the conservative cooling time, the final decay heat of the canister is determined as shown in Figure 3.4.

Table 3.2 Parameters for the decay heat model of PWR R-SNF after release from the nuclear power plant (Kim et al., 2021)

Parameter / Period	10<t≤100	100<t≤1000	1000<t≤100000
x_0	0.7805	101.65	863.15
y_0	297.95	32.19	1.01
t_1	2.94	40.56	32479.33
t_1	1.10	121.29	9417.81
t_1	42.75	622.19	622.70
A_1	3218.38	146.76	12.05
A_2	10394.94	110.40	20.78
A_3	2036.43	197.22	56.44

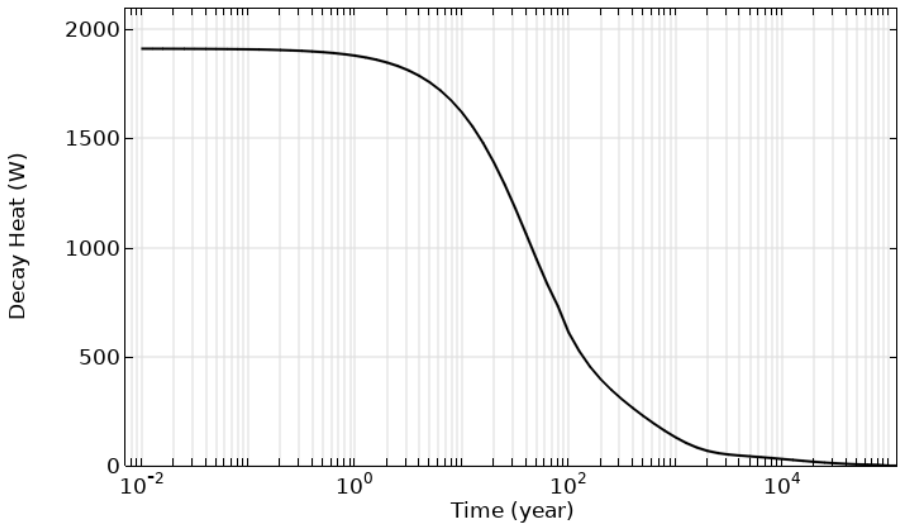

Figure 3.4 Decay heat of a high-level radioactive waste in a canister after disposal of the PWR R-SNF

Using the same decay heat model of spent fuel, the temperature of the near-field and far-field models was compared at the same depth of 250 m (Figure 3.5). The both models achieved the maximum temperature, approximately 32 ℃, at similar times. Although a temperature difference of 1–2 ℃ was observed between the near-field and far-field models during the cooling down of the rock mass, the temperature evolution was relatively similar in both models.

Even at the disposal level (500 m depth), the temperature evolution in the far-field model was similar to that of the host rock in the near-field model. The maximum temperature observed in both the far-field and near field models at similar depths was approximately 58 ℃. The temperature evolution along the vertical line of the rock mass in the near-field model was also similar to that of the far-field model. Therefore, in terms of the far-field scale, the constructed disposal system in the 3D far-field model can reveal the coupled THM behavior of the rock mass around the geological repository during long-term period.

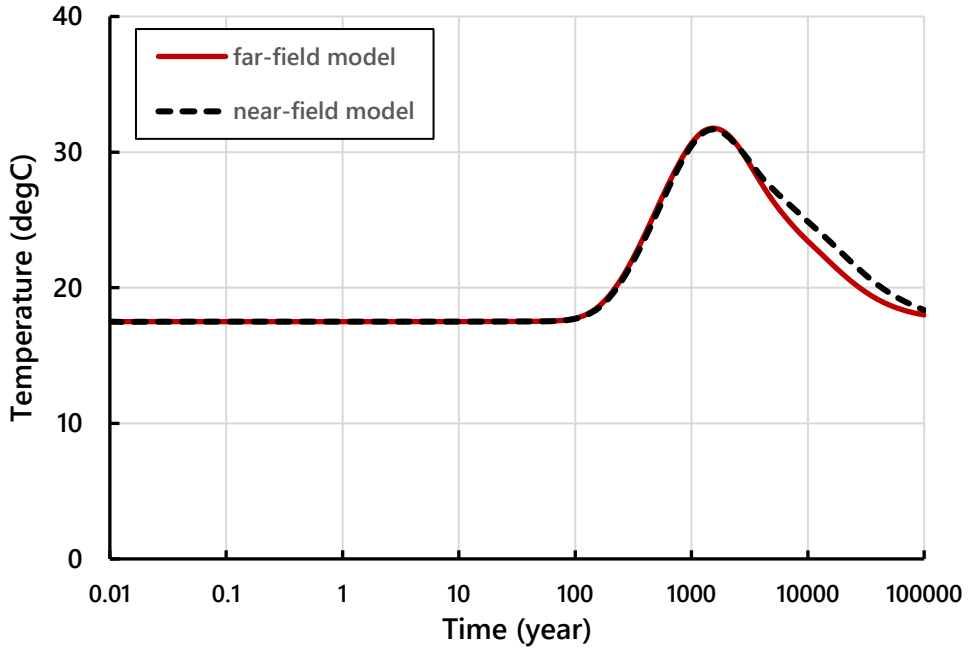

Figure 3.5 Comparison of the temperature evolutions in a point at a same depth of 250 m both in the near-field model and the far-field model

3.2.2 Alternative disposal systems

The estimated disposal area of the reference disposal system is approximately 5 km^2, which is larger than the area of Yeouido, Korea. Various alternative disposal concepts have been proposed to reduce the disposal area. There are several types of alternative disposal system, including multi-layered, multi-canister, and deep borehole disposal concepts. Particularly, in this study, three alternative disposal concepts (double-layered, triple-layered, and double-canister disposal concepts) were modelled and compared to the reference disposal system.

In the multi-layered disposal concept, the spacing between each layer was set to 200 m, according to the results of Lee et al. (2020a). The tunnel spacing and the hole spacing were adjusted differently for each alternative disposal concept according to the thermal analysis results of the near-field model (Figure 3.6). These thermal analyses were based on the assumption of a fully-saturated condition; thus, the real-life temperature evolution with consideration of the ventilation and excavation effects will be lower than these results. To determine the tunnel spacing and the deposition hole spacing, the thermal condition to ensure that the maximum temperature at the center of a canister should not exceed 100 ℃ was applied.

(a)

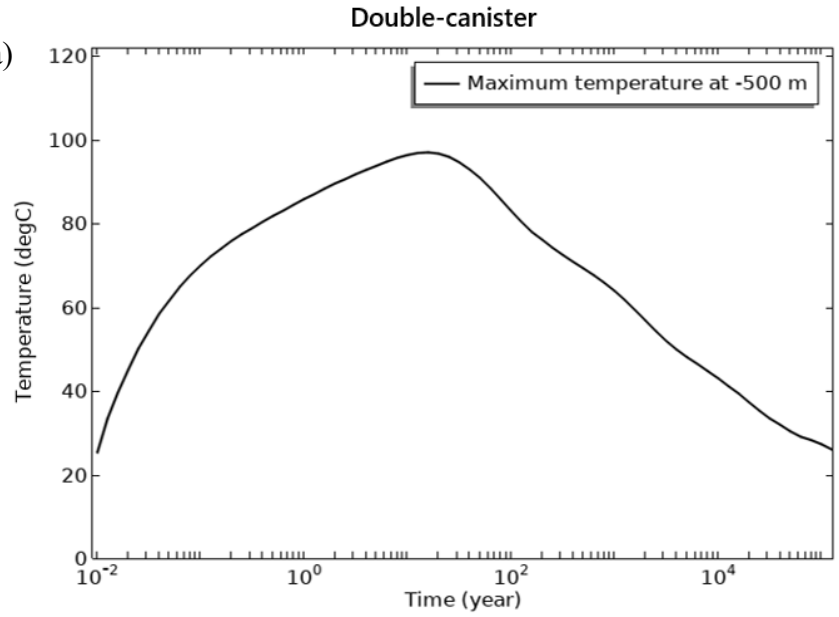
Double-canister
Maximum temperature at -500 m
Temperature (degC)
Time (year)
0
20
40
60
80
100
120
10-2
100
102
104

(b)

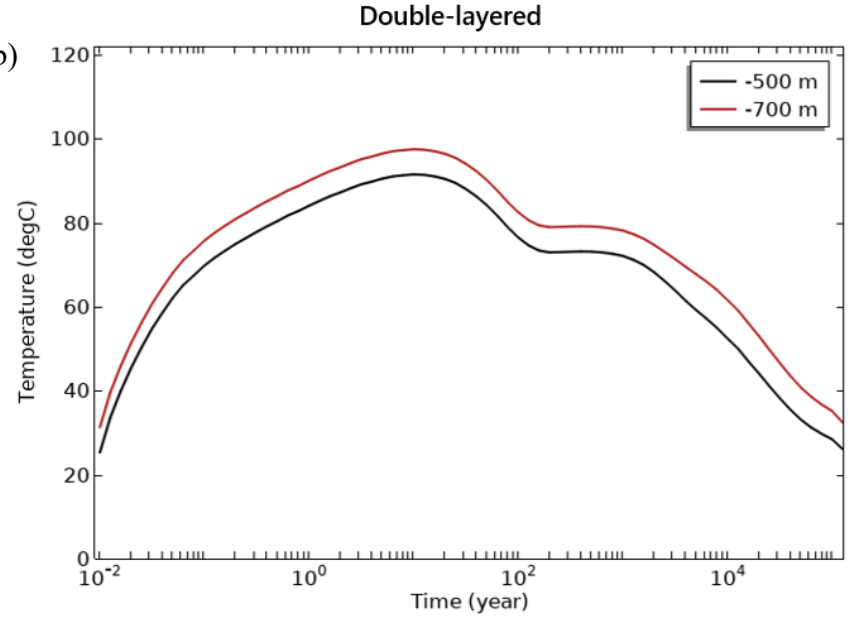
Double-layered
-500 m
-700 m
Temperature (degC)
Time (year)
0
20
40
60
80
100
120
10-2
100
102
104

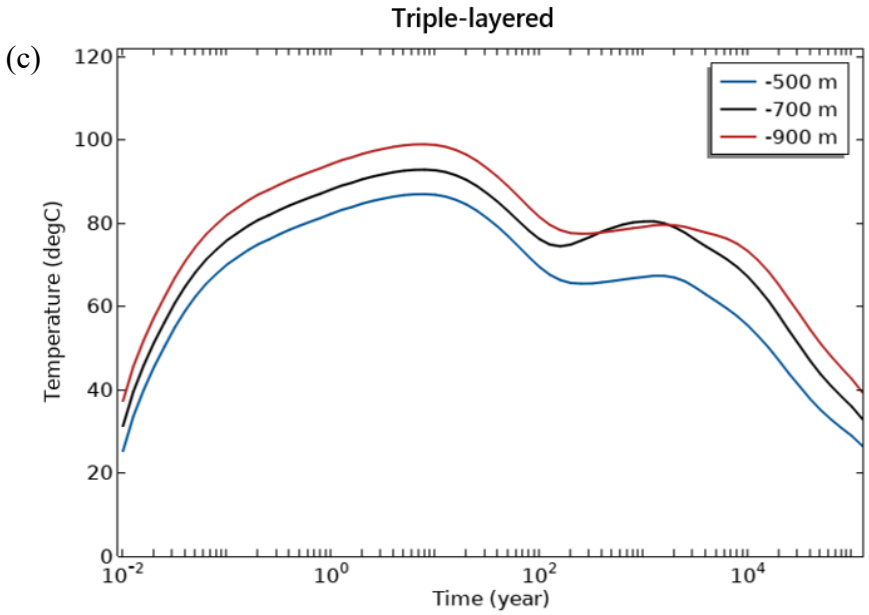

Figure 3.6 Temperature evolution from thermal analysis for each alternative disposal concept; (a) Double canister (b) Double-layered (c) Triple-layered

The tunnel spacing of all the modelled disposal concepts was 40 m. The hole spacing of the double canister repository was set to 13 m, whereas that of the double-layered and triple-layered repository was set to 8 and 10 m, respectively.

As the reference disposal system, the number of the canisters in a quarter disposal system was set to 3,750. It was assumed that 1,875 canisters will be disposed in a layer of the double-layered disposal system, whereas 1,250 canisters will be disposed in a layer of the triple-layered disposal system. Based on the number of canisters and the spacing between the tunnels and holes, the equal disposal area of each disposal concept was determined (Figure

3.7). Compared to that of the reference disposal system, the area of the geological repository of all the alternative disposal systems would be largely decreased (Table 3.3).

Table 3.3 Spacing values and reduction of disposal area in each disposal system

Disposal concept	**Reference**	**Double-canister**	**Double-layer**	**Triple-layer**
Disposal depth	-500 m	-500 m	-500 m -700 m	-500 m -700 m -900 m
Tunnel spacing (m)	40	40	40	40
Hole spacing (m)	7.5	13	8	10
Quarter of disposal area	1.125 km^2	0.975 km^2	0.6 km^2	0.5 km^2
Ratio of disposal area	**100 %**	**87 %**	**53 %**	**44 %**

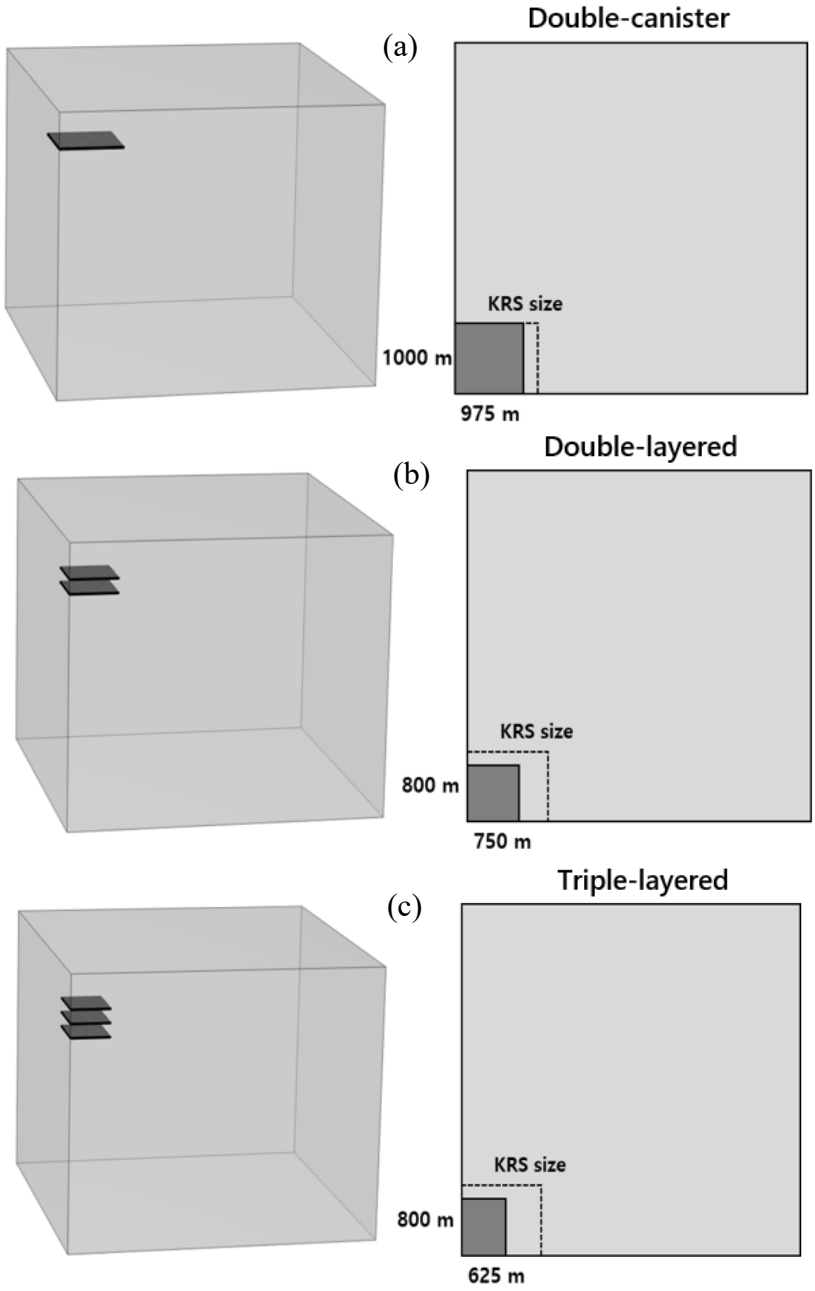

Figure 3.7 3D numerical geometry and xy-plane to show the size of each alternative disposal systems (a) double-canister (b) double-layered (c) triple-layered

3.3 Input parameters, initial and boundary conditions

The far-field numerical model was constructed as a symmetric quarter model of an entire disposal system. Thus, except the top of the model, all the boundaries were applied to the roller boundary condition (Figure 3.8). At the top and bottom of the model, the initial and boundary conditions were applied at a constant pressure and temperature. In addition, the temperature at the top and bottom of the model was fixed at 10 ℃ and 130 ℃, respectively. Similarly, the pore pressure at the top and the bottom of the model was fixed at 0.1 MPa and 39.34 MPa, respectively. The initial temperature distribution followed the geothermal gradient, as described in Eq. (3.2) under the assumption of a geothermal gradient of 30 ℃/km.

$$T = 10 + 0.03 \times (-z\ [1/m])\ \ (Unit: ℃) \tag{3.2}$$

The initial pressure follows the hydrostatic pressure distribution as described in the following (Eq. (3.3)).

$$p = -0.00981 \times (-z\ [1/m]) + 0.1\ \ (Unit: MPa) \tag{3.3}$$

In this research, the excavation and the ventilation effect were not considered for simplicity. This is justified as the focus of the current study is the middle- to far-field influences of thermally induced stress on nearby faults.

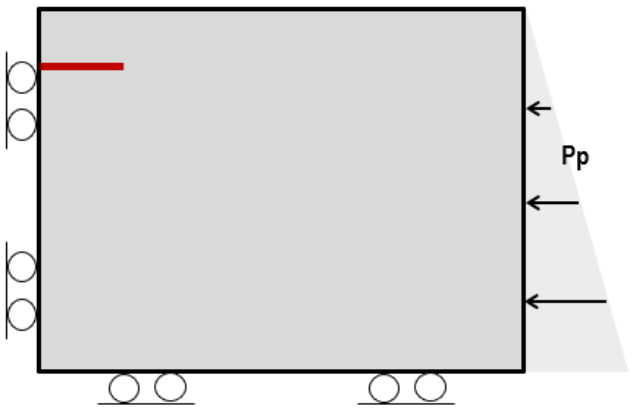

Figure 3.8 Scheme depicting boundary conditions on 3D numerical far-field model

The input properties used for the THM simulation were obtained from the study of Lee et al. (2020a). In the near-field model, the input parameters of the canister, buffer, and backfill were used. In contrast, in the far-field model, only the properties of the rock mass were used for the THM simulation, as is shown in Table 3.4. This is because the disposal area mostly consisted of the rock mass, in other words, the properties of the canister, buffer, and backfill can be considered as negligible. Here, the thermal expansion coefficient of the rock mass is expressed as a function of temperature as follows (Lee et al., 2019):

$$\alpha = 0.7704\sqrt{T} + 1.3306) \times 10^{-6} \quad (3.4)$$

Table 3.4 Input properties of rock mass

Properties	**Value**
Density (kg/ m^3)	2650
Poisson's ratio	0.3
Elastic modulus (GPa)	32.8
Saturated thermal conductivity (W/m/K)	3.31
Heat capacity (J/m/K)	820
Permeability (m^2)	1.0×10^{-18}
porosity	0.0116
Thermal expansion coefficient (1/K)	Eq. (3.4)

Chapter 4. Thermal, hydraulic and mechanical response around the geological repository

4.1 Thermal behavior

The thermal behaviors of the reference and alternative disposal systems are described in this section. The initial temperature in all the disposal systems was set to be the same, and the temperature evolutions at the center of each disposal system over time are presented in Figure 4.1. The maximum temperature of the rock mass in the reference disposal system was approximately 58.9 ℃ after 125 years. Considering that the initial temperature at a depth of 500 m was 25 ℃, the result indicated that the temperature increased by more than 30 ℃ owing to decay heat. This highly increased temperature will be mostly maintained for 1,000 years, after which it will decreases gradually. Even after a long time, such as 100,000 years, a temperature increase of approximately 10 ℃ was maintained.

The temperature evolution in the double-canister disposal system over time was almost the same as that of the reference disposal system, but the maximum observed temperature was slightly higher by approximately 5 ℃. In contrast, the temperature evolution at each disposal layer of the multi-layered disposal systems was different from that of the reference disposal

system. In addition, the time taken by this system to achieve the maximum temperature was delayed by 1,000 years compared to that of the reference disposal system. Furthermore, the peak temperature of the second disposal layer in the triple-layered system was significantly higher than those of other layers from 300 years to 2,000 years. This indicates that it essential to carefully investigate the temperature increase in the second layer of the triple-layered alternative disposal system.

The temperature distribution along the vertical line at the center of each disposal system is shown in Figure 4.2. Compared to the reference disposal system, there were notable differences in the temperature distribution in the multi-layered disposal system. The change in temperature at each layer in the double-layered disposal system was the same; however, the increase in the temperature at the second layer in the triple-layered disposal system was higher. Thermal effect due to decay heat from the spent fuel heated the rock mass and the increase in the temperature was affected upward and downward. Thus, thermal effect from up and down overlapped at the middle layer in the tripled-layered disposal system, and this may be the reason for the observed maximum temperature at the second layer in the triple-layered disposal system compared to the double-layered disposal system. Although the amount of the decay heat from each layer was lower than that of other disposal concepts, the final temperature change was the largest, so attention should be paid to this thermal behavior.

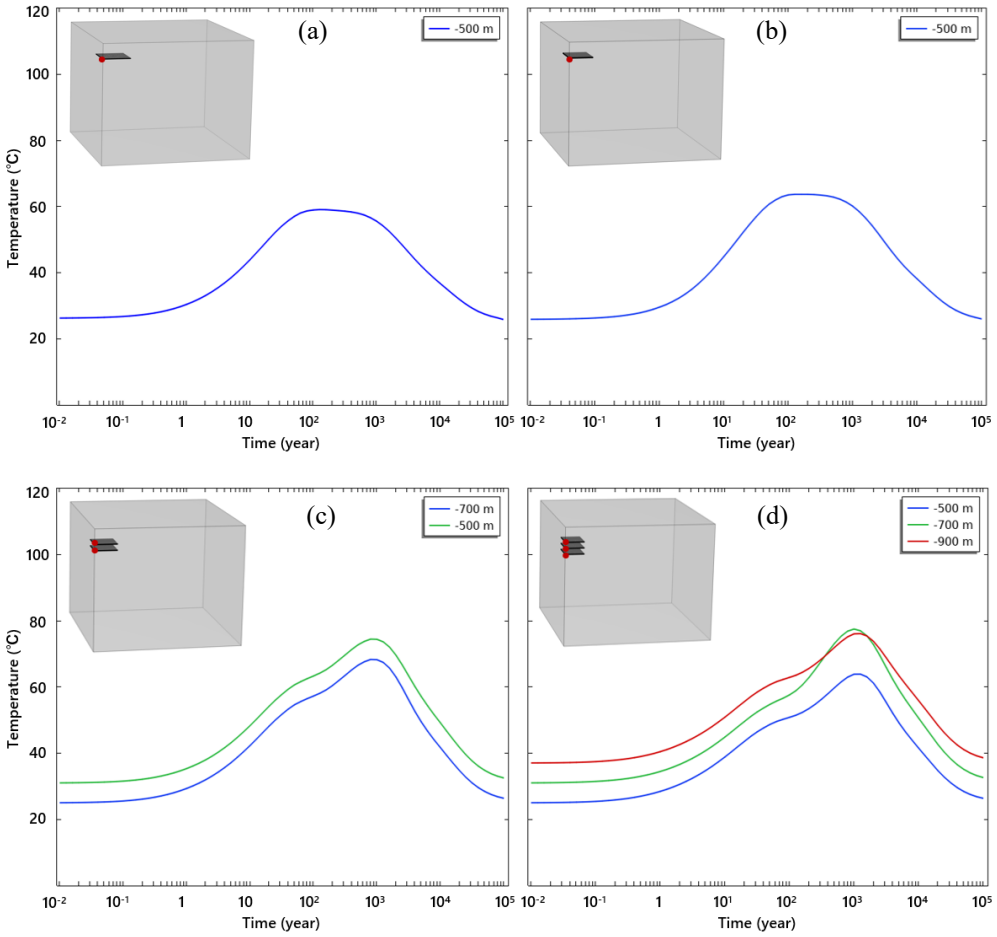

Figure 4.1. Temperature evolutions at a point in the center of each disposal system at the disposal depth (a) Reference (b) Double-canister (c) Double-layered (d) Triple-layered

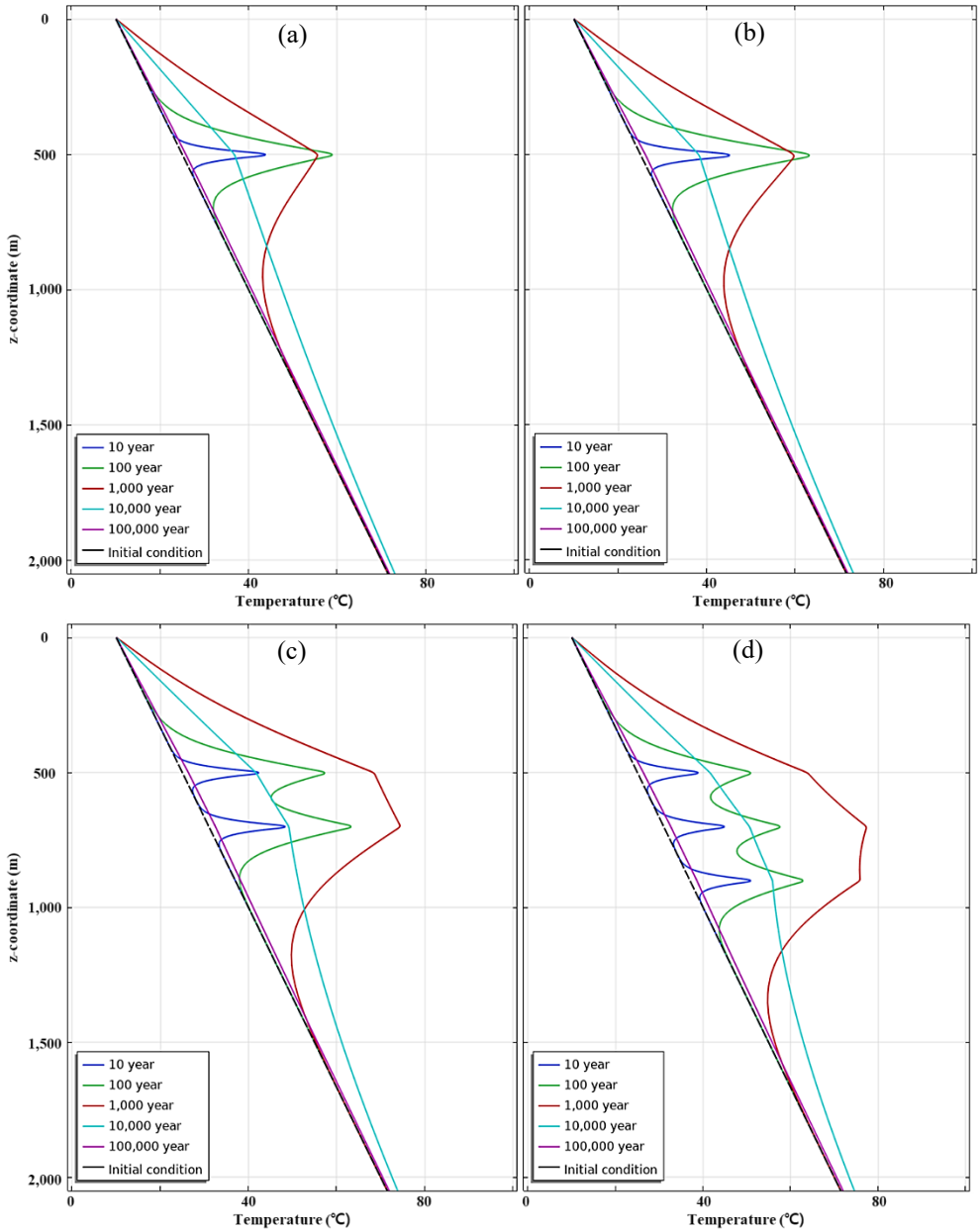

Figure 4.2 Temperature distribution along the vertical line through the center of each disposal system (a) Reference (b) Double-canister (c) Double-layered (d) Triple-layered

4.2 Hydraulic behavior

Next, the hydraulic behavior in each disposal system was investigated. A fully water saturated condition was considered as the initial condition. As mentioned in section 2.1, owing to the thermal pressurization in the low-permeability porous media, an increase in the pore pressure was observed in all the disposal systems (Figure 4.3). In the reference disposal system, the pore pressure at the center of the geological repository increased by 3.5 MPa, and the pore pressure increase was transferred to the above and below regions of the geological repository. Additionally, the reference disposal system could maintain the residual increase in the pore pressure after a very long time of approximately 10,000 years. When the effective stresses were considered in evaluating the possibility of the fault reactivation, the increased pore pressure of the rock mass around the geological repository would increase the possibility of the fault reactivation

The pore pressure evolution in the double-canister disposal system was almost similar to that of the reference disposal system. However, at the disposal level, the pore pressure increased by 4.3 MPa, which was higher than that of the reference disposal system. In the multi-layered disposal system, pore pressure increased along each layer; however, the pattern of the pore pressure increase after 100 years was similar to those of the reference and double-canister disposal systems. With an increase in the depth of the disposal

layer to 900 m in the triple-layered disposal system, the range of the increase in the pore pressure appeared to be deeper and larger than those of the other disposal systems. The maximum increase in the pore pressure in the double-layered and triple-layered disposal systems was 5.6 and 6 MPa, respectively. Compared to single-layered disposal system, such as the reference and double-canister disposal systems, the maximum increase in the pore pressure in the multi-layered disposal systems was observed between layers. The maximum increase in the pore pressure of the double-layered and triple-layered disposal systems was observed at a depth of 575 and 650 m, respectively.

During heating, the porosity and permeability decreased with a change in the volumetric strain. After the maximum temperature was achieved, the hydraulic properties of the disposal systems returned almost to the initial values. As the saturation change was not considered in this hydraulic analysis, only the fully saturated condition was assumed. Thus, these results are based on ideally fully saturated porous continuum media and just only the overall pore pressure change was investigated for the assessment of the fault reactivation, which will be discussed in the next chapter.

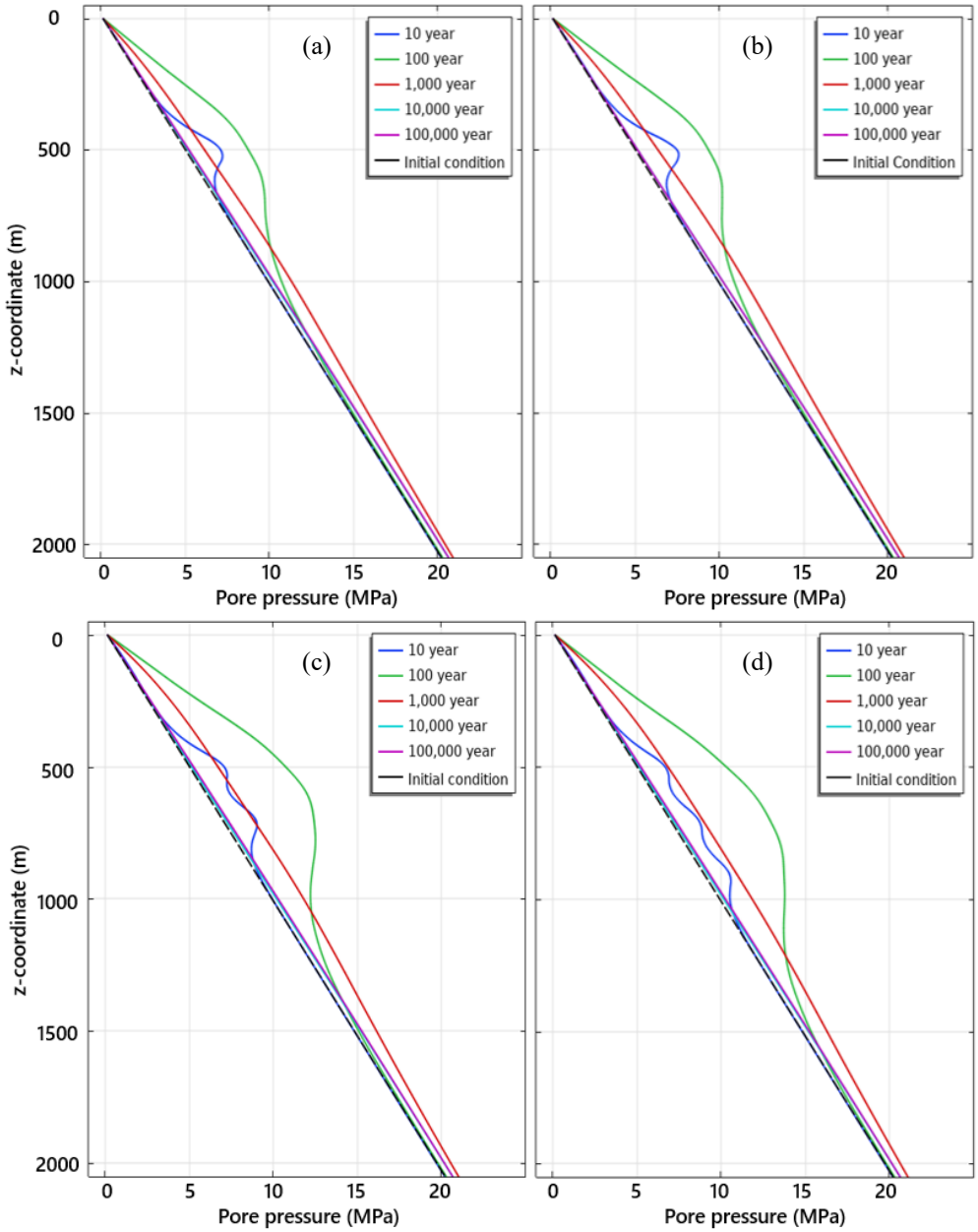

Figure 4.3 Pore pressure distribution along the vertical line through the center of each disposal system (a) Reference (b) Double-canister (c) Double-layered (d) Triple-layered

4.3 Thermal stress generation

Owing to the decay heat from the spent nuclear fuel, thermal stresses are generated around the geological repository. Particularly, horizontal stresses are largely generated inside the geological repository, whereas tensile stresses are generated above the geological repository. Over time, the tensile stress is transferred to the ground surface, thus the maximum tensile stresses are observed after hundreds to thousands of years. The mechanism involved in the thermal stress generation and thermal stress evolutions at different depth and distance in a single-layered disposal system are extensively discussed by Min et al. (2013).

In this study, the thermal stress generation of the multi-layered and double-canister disposal systems, as well as for the reference disposal system, was analyzed. In the far-field scale, the thermal stress evolutions in the double-canister and reference disposal systems were almost similar. The only difference is that the generated compressive thermal stress in the middle of double-canister disposal system was larger (30 MPa). The 3D colored contours of the generated thermal stresses in the reference and double-layered disposal systems are representatively shown in Figure 4.4. The overall stress distribution in the multi-layered disposal system exhibited a similar trend with that of the reference disposal system as smaller thermal stress was generated. In the double- and triple-layered disposal systems, the maximum compressive

stresses (26 and 25.7 MPa, respectively) were observed in the second layer. In addition, compared to those of the reference and the double-canister disposal systems, the tensile stress at the ground surface of the multi-layered disposal system was significantly higher. Furthermore, compared to the maximum generated tensile stress in the reference disposal system (approximately 8 MPa), the maximum generated tensile stress in the triple-layered disposal system was 18 MPa, which was 2 MPa higher than the maximum value of the double-layer disposal system. Although the area occupied by the geological repository in the alternative disposal system was obviously reduced, it seemed that the tensile stress generation at the ground surface was significantly larger because the effect of the heat source is concentrated at the center of the geological repository.

The compressive vertical stress was generated and increased within the disposal area at the early time until approximately 100 years. After reaching the maximum value, it decreased gradually and returned to the initial state. However, the tensile vertical stress was generated near the boundary of the disposal system up to a few hundreds of meters until 100 years, after which it gradually recovered to the initial state. During recovery to the initial state after 100 years, the magnitude of the tensile vertical stress decreased, but its region extended farther away to approximately 2,000 m. The compressive vertical stress was generated more deeply in the multi-layered disposal system. Regarding the shear stress, it was mainly generated at the corner of the

geological repository. The shear stress was generated in the opposite directions above and below the boundary of the geological repository. This indicates that the direction of the shear slip above and below the geological repository can be different. In the multi-layered disposal system, it increased above the first layer and decreased at the bottom layer with a transition zone between the layers

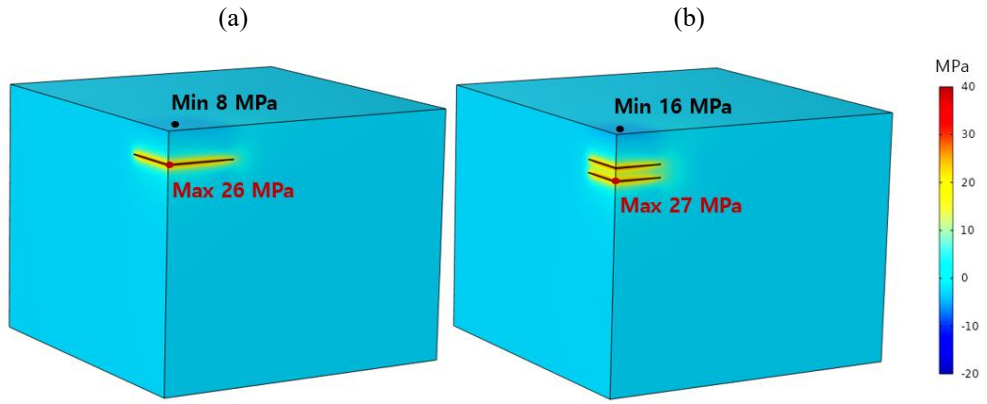

x-direction normal stress

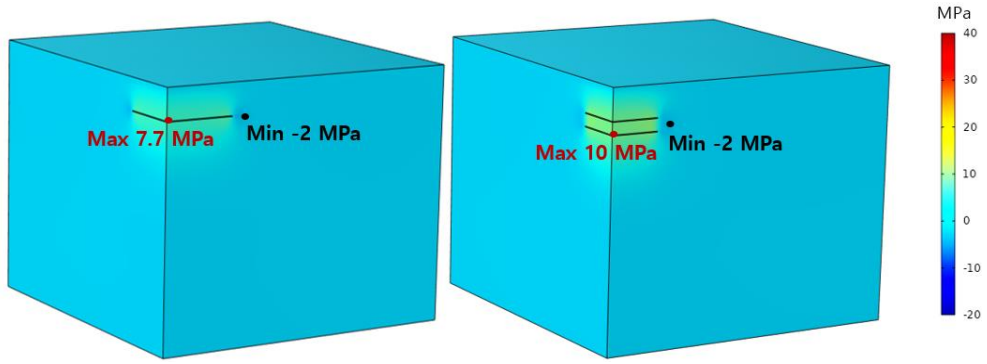

z-direction normal stress

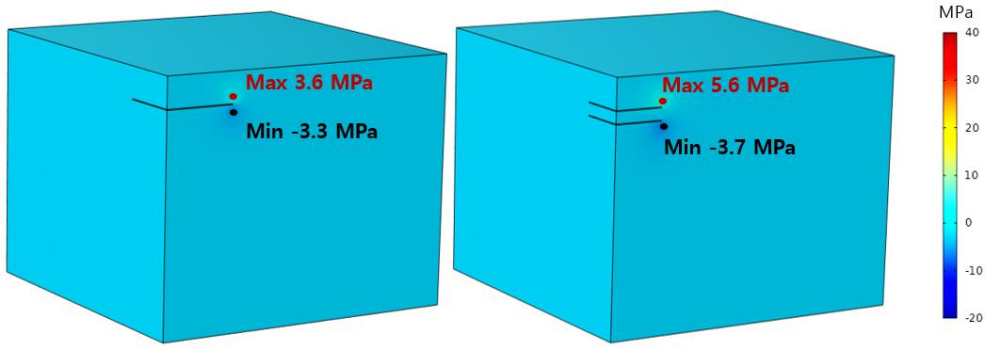

xz-direction shear stress

Figure 4.4 Thermal stresses including x-direction horizontal stress, z-direction vertical stress, and xz-direction shear stress distribution on the 3D colored contour after 100 years in (a) the reference disposal system and (b) the double-layered disposal system

4.4 Ground heaving by thermal effect

The thermal expansion of the rock mass due to decay heat induced ground heaving at the surface above the geological repository. Thermal expansion occurred at a depth of 500 m, after which heat was transferred to the surface over a long period of time. Thus, after more than 1,000 years of the disposal of the spent nuclear waste, a maximum ground uplift was observed. In this section, the evolution of the ground uplift due to thermal effect of HLW was investigated with respect to various disposal concepts.

Among all the disposal systems, the multi-layered disposal system generated the highest maximum ground uplift (Figure 4.5(a)) in the center of the surface. The maximum surface uplift values of the double-layered, triple-layered, double-canister, and reference disposal systems were 0.43, 0.42, 0.33, and 0.31 m, respectively. The maximum ground uplift in the reference, double-layered, and double-canister disposal systems was achieved after approximately 1,500 years, whereas the time was delayed for approximately 400 years in the triple-layered disposal system. Although these maximum values of several tens of centimeters seem quite large, it will proceed slowly for more than 1,500 years. Therefore, these ground uplift of the disposal systems might not be so threatening.

The maximum ground uplift is largely affected by the presence of layers in the disposal system. In the multi-layered disposal system, the maximum

ground uplift was approximately 10 cm larger than those of the reference and double-canister disposal systems, which are single-layer disposal systems. The maximum value of ground uplift in the double- and triple-layered disposal systems appeared to be almost the same, but was slightly larger in the double-layered disposal system. However, this slight increase can be considered negligible as it reduced over time.

The ground uplift distribution along the x-direction shown in figure 4.5(b) indicates that the ground uplift occurs to a slightly greater distance from the double-layered disposal system. Additionally, below the lower layer, the increase in the vertical displacement gradually decreased and the increase in the vertical displacement moved upward in the area above the first layer. The maximum vertical displacement was observed at a depth of approximately 200 m. Consequently, when the disposal system has the same total amount of heat sources, the occurrence of ground uplift increased with a decrease in the disposal area. Particularly, the value increased significantly in the case of the multi-layered disposal systems.

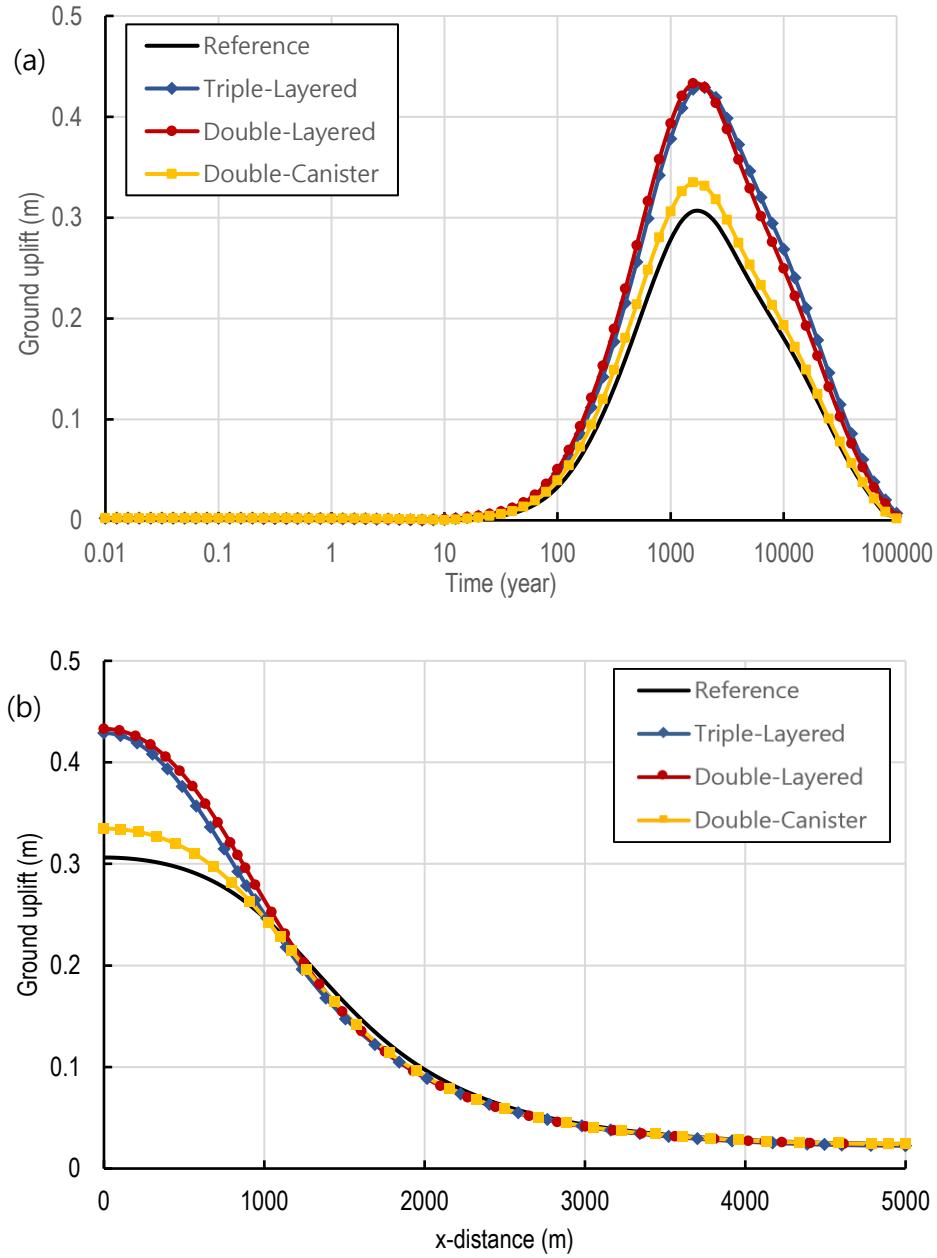

Figure 4.5 Ground heaving at different time and the different distance (a) Ground heaving evolution at different time (b) Ground heaving along the x-distance at the time which has the maximum ground heaving value in each disposal concept

When discussing the risk of ground heave or subsidence, not only the maximum value but also their angle and velocity are important. These values of each disposal concept are shown in Table 4.1. The maximum ground heave rate and angle were observed in double-layered disposal system. The comparison of the other two alternative models revealed that the ground heave velocity in the triple-layered system was faster, whereas the angle in the double-canister system was larger. This indicates that the double-layered systems exhibited a relatively high risk of ground heaving; however, as the overall heave velocity or angle of the uplift is very small, a question of whether the occurrence of ground heaving will imply a direct risk is remains to be investigated further.

Table 4.1 Ground heaving velocity and the maximum angle of each disposal concept

	Reference	**double-canister**	**double-layer**	**triple-layer**
Heave velocity (mm/year)	0.501	0.574	0.735	0.679
Maximum angle (°)	0.01	0.0148	0.0154	0.0112

Chapter 5. Assessment of fault reactivation

In this section, the possibility of the fault reactivation around the disposal systems was assessed by calculating the CFS change. The amount of CFS change was evaluated at a specific fault plane with a dip of 30° and a dip direction of 90°. To evaluate the possibility of the fault reactivation only according to decay heat from HLW, the amount of change in the normal stress and shear stress exerted on the fault plane was calculated. The friction coefficient of the fault to be used in calculating the CFS change in Eq. (2.6) was set to 0.6 as a reference value for conservative assessment.

5.1 CFS change of each disposal concept

To evaluate the risk of fault reactivation, the CFS change at a constant distance of 500 m from each disposal system was calculated, and the result is shown in Figure 5.1. For the reference and double-canister disposal systems, the results were plotted at a disposal depth of 500 m, whereas for the multi-layered disposal systems, the result of the 700 m depth was plotted as a solid line and the result of the 500 m depth was plotted as a dashed line. The results revealed that the triple-layered disposal system exhibited the highest possibility of fault reactivation. In addition, compared to those of the reference

and the double-canister disposal systems, the CFS of the multi-layered disposal systems increased by more than 1–2 MPa. Furthermore, the temperature of the multi-layered disposal system increased, and was maintained for a long time owing to the superposition effect of the decay heat of different layers. This may also have contributed to the increase in the risk of fault reactivation in the vicinity of the disposal system. At a depth of 500 m, the double-layered disposal system exhibited the largest the CFS change, as plotted in the red dashed line. This indicates that the possibility of fault reactivation in the multi-layered disposal system differed depending on the depth.

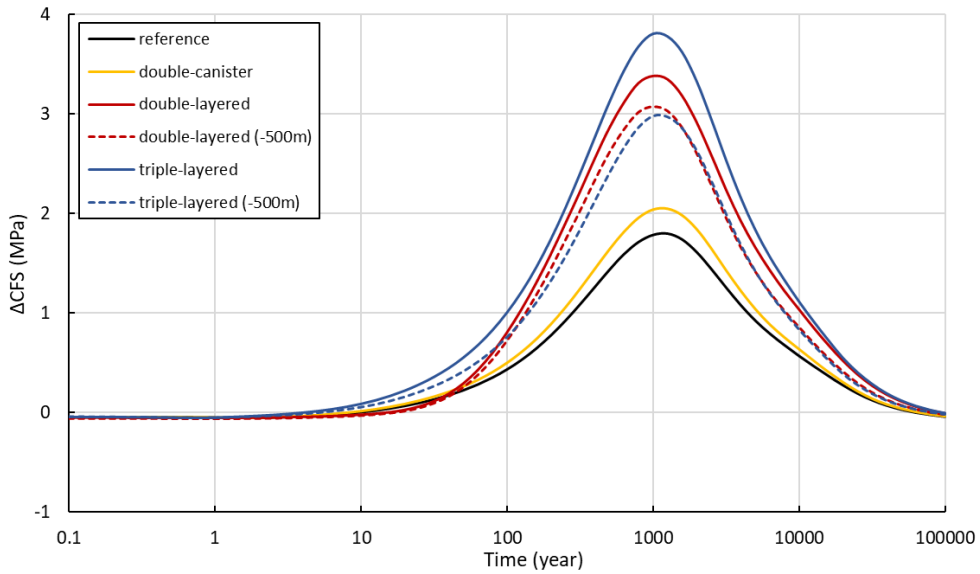

Figure 5.1 The CFS evolutions with time at a distance of 500 m away from the boundary of each disposal system

The CFS changes in each disposal system along the x-direction at different time steps are presented in Figure 5.2. This figure shows the CFS change according to the distance from the disposal systems because this research aimed to assess the possibility of fault reactivation around the geological repository not inside the geological repository. The CFS change by 0.01 MPa was also plotted as a criterion in a dashed line. The CFS change in the reference and double-canister disposal systems was analyzed at a depth of 500 m, whereas that of the multi-layered disposal systems was analyzed at a depth of 700 m. This is because the largest thermal stress was observed in the multi-layered disposal systems at a depth of 700 m owing to the superposition of decay heat

At the early time period, after the disposal of HLW, the CFS change increased significantly, but the range did not exceed 1,000 m in all the disposal systems. Until 100 years, the CFS change was positive only within 1,000 m of the disposal system, suggesting that the fault at a distance further than 1,000 m is still in a stable state. This is because the thermal stress exerted no effect on farther distances at the early time. In the reference and double-canister disposal systems, the CFS change gradually starts to decrease after 100 years, but a positive CFS change was still observed further away from the disposal system (Figure 5.2 (a) and (b)). In contrast, the CFS in the multi-layered disposal systems increased even after 100 years, and reached its maximum value after approximately 500 years, after which it started to decrease (Figure

5.2 (c) and (d)). The maximum CFS increases are observed as 4.2, 4.9, 5.3, and 5.6 MPa in the reference, double-canister, double-layered, and triple-layered disposal system.

It was observed that the maximum CFS change was not just at the boundary of the disposal system, but at a distance of 50 m in the single-layered disposal system and a distance of 200 m in the multi-layered disposal systems. The pattern of these CFS change seemed to be significantly affected by the vertical stress. As mentioned in the previous chapter, the tensile vertical stress occurred up to a few hundred of meters from the boundary of the disposal system. This could be the reason for the increase in the possibility of fault reactivation as the tensile vertical stress was generated, whereas the compressive horizontal stress was generated with the reverse stress regime.

Even after 10,000 years, a CFS change larger than 0.01 MPa was generated up to 3 km away from the disposal boundary. From a distance of 3,360 m, the CFS change in the reference disposal system was smaller than 0.01 MPa. In the double-canister, double-layered, and triple-layered disposal systems, the CFS change decreased to less than 0.01 MPa from a distance of 3,497, 3,538, and 3,828 m, respectively. These results suggest that if there is a critically-stressed fault with a dip of 30° and a dip direction of 90° at a distance of approximately 3,000 m from the geological repository, it can be more stable at the early time of the geological repository operation, but there could be an increased risk of fault slip after a long time of approximately 10,000 years.

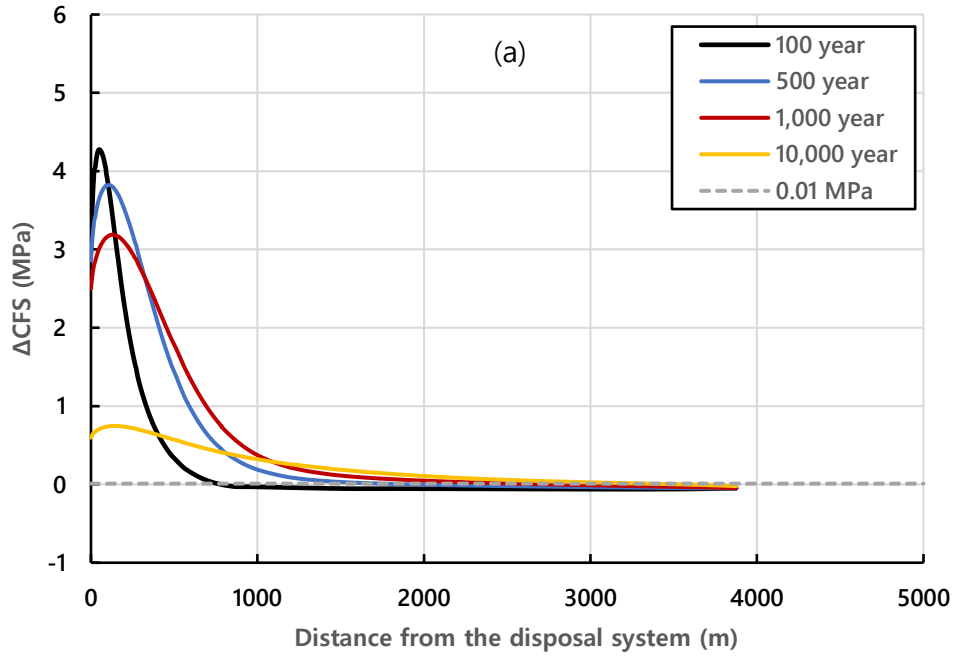
(a)
100 year
500 year
1,000 year
10,000 year
0.01 MPa
ΔCFS (MPa)
6
5
4
3
2
1
0
-1
0
1000
2000
3000
4000
5000
Distance from the disposal system (m)

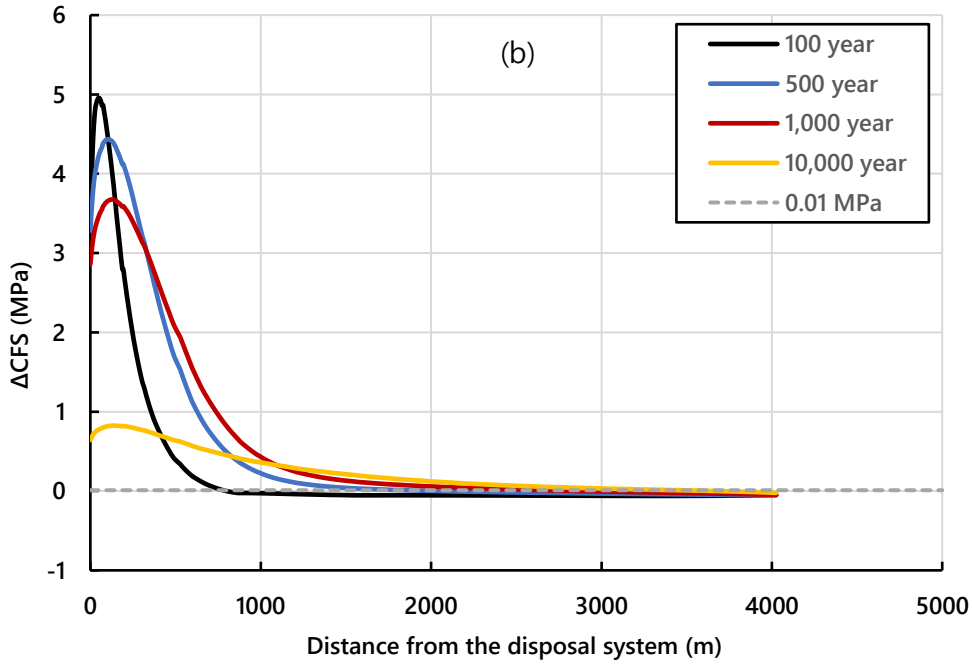
(b)
100 year
500 year
1,000 year
10,000 year
0.01 MPa
ΔCFS (MPa)
6
5
4
3
2
1
0
-1
0
1000
2000
3000
4000
5000
Distance from the disposal system (m)

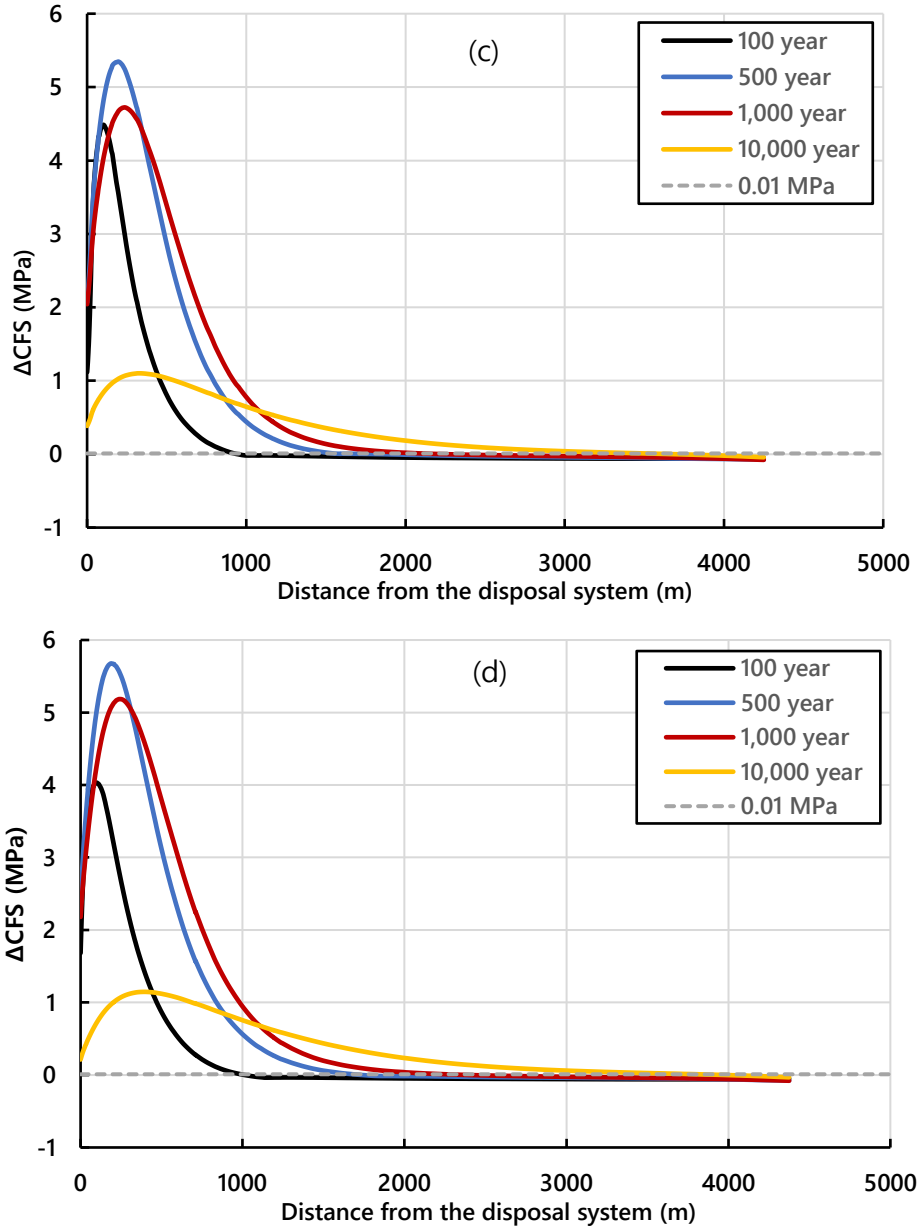

Figure 5.2 CFS evolutions along the x-distance from the disposal system; (a) reference (b) Double-canister (-500 m) (c) Double-layered (-700 m) (d) Triple-layered (-700 m)

To analyze the disposal depth, as well as the overall possibility of fault reactivation around the reference disposal system, the CFS change according to each different time step is shown as a colored 3D contour (Figure 5.3). There were three sections where the CFS change increased significantly around the geological repository: inside the geological repository, near the boundary at the disposal depth, and the ground surface above the disposal system. First, as described in the previous section, the compressive horizontal stresses inside the geological repository were large, but the increase in the vertical stress was relatively smaller. Accordingly, as the size of the Mohr's circle increased, a positive CFS change was observed, which will be the main cause of the fault reactivation inside the geological repository. Next, the CFS change near the boundary at the disposal depth increased with an increase in the generation of tensile vertical stress, as described previously. Lastly, at the ground surface above the disposal system, the initial stress state will typically be zero or very small. In such a stress state, as the horizontal tensile stresses are generated significantly, the risk of the fault reactivation with the fracture opening increased.

In addition to the places where CFS increased intensively, complex CFS change patterns were observed around the disposal system owing to factors, such as complex thermal stress generation and changes in the principal stresses directions. At some places, such as intermediate depths between the ground surface and the disposal system, below the disposal system, and in the region

rising to the surface diagonally from the boundary of the disposal system, the CFS decreased, indicating the stabilization of the fault. Particularly, after a very long period of time, such as 10,000 years, the extent of negative CFS reached approximately 2,000 m depth.

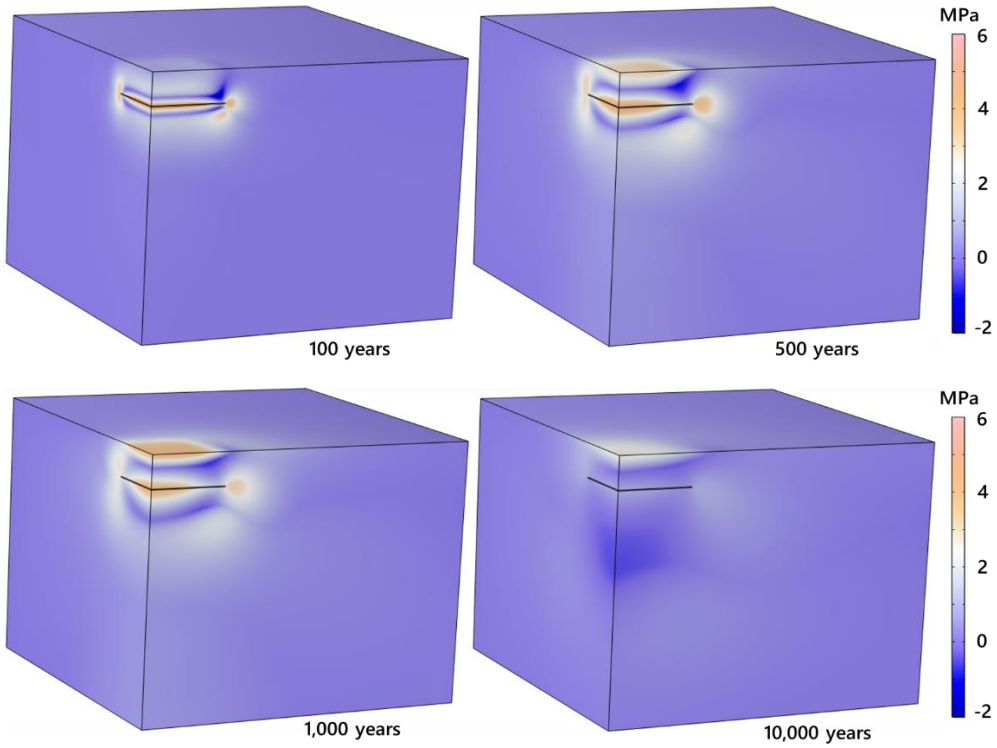

Figure 5.3 Distribution of CFS change at different time step in the reference disposal system

The distribution of the CFS change at 100 and 500 years in the alternative disposal systems are presented in Figure 5.4. Notable anisotropic CFS change was observed in all the disposal systems. This anisotropy CFS change seems to have occurred not only because of the anisotropic thermal stress generated

at the boundary of the disposal system but also because the principal direction of the stress acting on the fault plane changed with the generation of thermal stress. In the double-layered disposal system, CFS quite increased even between layers. Otherwise, The CFS significantly decreased upward and downward of the disposal layers. It indicates that the possibility of fault reactivation between the disposal layers increased in the early time, but the side, bottom, and top of the disposal system could be more dangerous, as time goes on. In the triple-layered disposal system, the initial increase in the possibility of fault reactivation between disposal layers is similar to the double-layered disposal system. However, it was observed that the fault rapidly stabilized from the boundary of the disposal system to the center. Consequently, as the CFS increased to the top, center, boundary side, and bottom of the entire disposal system, it is necessary to monitor these parts.

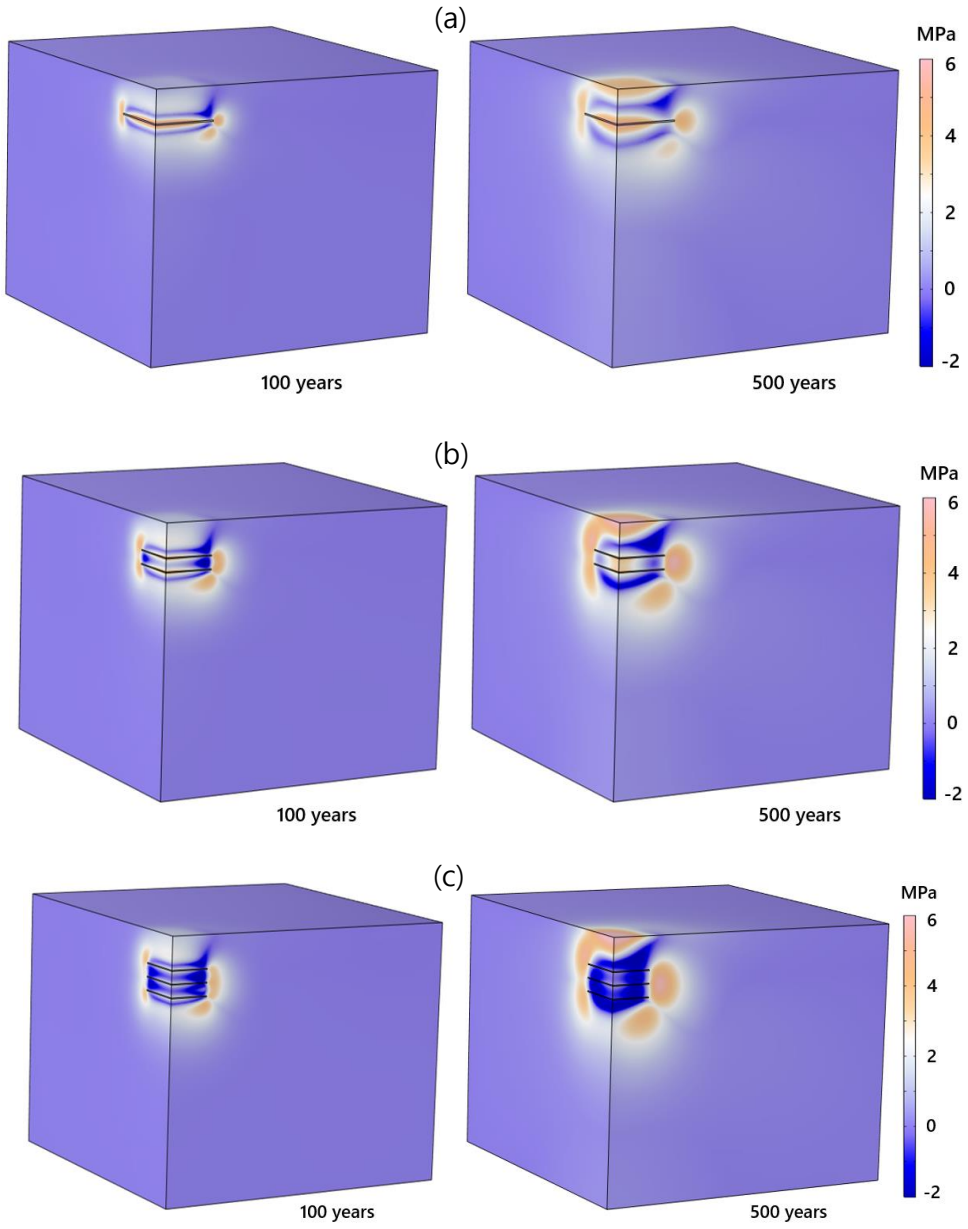

Figure 5.4 Distribution of CFS change at different time step in the alternative disposal systems (a) Double-canister (b) Double-layered (c) Triple-layered disposal system

5.2 Effect of the fault orientation on CFS change

The CFS change of the faults at various dips and dip directions was analyzed, and the results were presented using the stereonet upper equal area projection method. Therefore, the CFS change on the different fault direction could be analyzed at several points near the disposal systems.

Figure 5.5 shows the stereonets of the projected CFS changes in the reference disposal system over time at three different points. The CFS change at point R-A, which is a center of the disposal system shown in Figure 5.5 (a), is presented in Figure 5.5 (b). Here, the dip of the fault, rather than the dip direction of the fault, exerted a major influence on the fault reactivation. This is because the compressive thermal stresses were largely generated in both the x- and y-directions at the center of the disposal system. It seems that the CFS increased even in the case of a fault with a dip of approximately 60° from a near-horizontal fault plane regardless of the direction of the fault plane. However, in the vicinity of the boundary, the dip direction of the fault may also affect the possibility of the fault reactivation. At point R-B, which is at a distance of 50 m from the boundary of the disposal system, the highest CFS change was observed when the dip of the fault was approximately 30° and the dip directions were 90 and 180° after 100 years (Figure 5.5 (c)). Thereafter, the region where CFS increased with time decreased mainly along the N-S

direction; however, the maximum change was still observed when the dip and the dip direction were similar to those at 100 years. The stereonet at point R-C with a distance of approximately 300 m from the inner boundary of the disposal system inside the numerical model is shown in Figure 5.5 (d). Compared to the previously discussed points, the principal thermal stress direction rotated as the thermal stress was generated in the xy-direction. Accordingly, the maximum CFS appeared mainly in the NW direction faults, and an increase of more than 1.5 MPa in the CFS was observed even after 1,000 years.

In this study, fault reactivation was analyzed under the assumption that there is no information on the initial stress state by considering only the changes in the normal stress and shear stress acting on the fault plane. Therefore, s1, s2, and s3 indicated on the stereonet are not the real principal stress directions, but the principal stress directions of the thermal stresses generated only according to the decay heat of the spent nuclear fuel regardless of the initial stress.

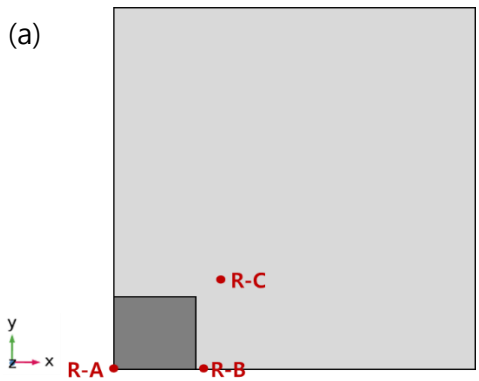

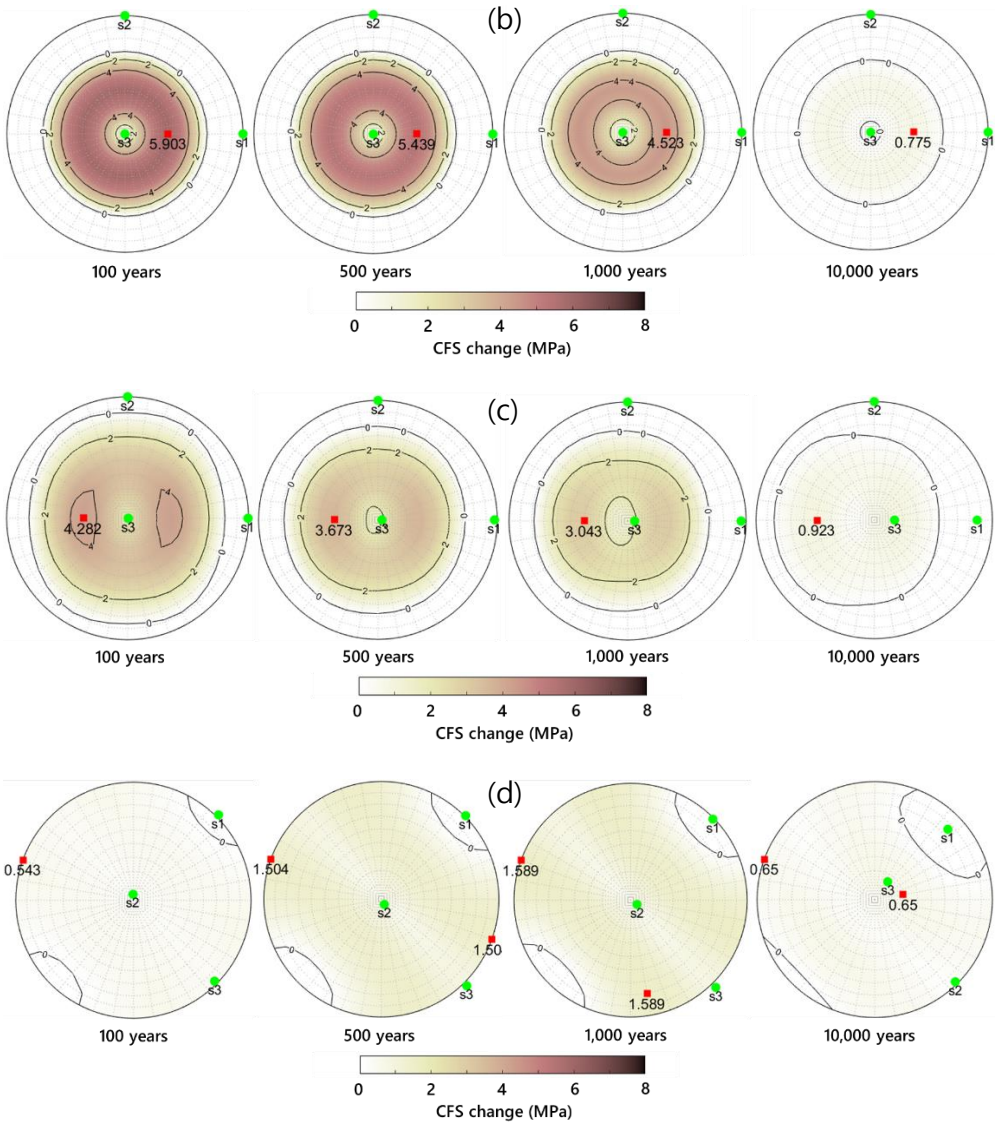

Figure 5.5 Evolution of CFS change with time in the reference disposal system, showing the direction of principal thermal stresses as green colored points and the maximum CFS change as red colored points (a) Position of the monitoring points (b) point R-A (0, 0, -500) (c) point R-B (1175, 0, -500) (d) point R-C (1325, 1200, -500)

In the double-canister disposal system, as the generation of thermal stress around the double-canister disposal was almost similar to that of the reference disposal system, only the CFS change at a distance of 200 m from the boundary at the disposal depth was plotted in the stereonet (Figure 5.6). Initially, after 100 years, a maximum value of approximately 2.7 MPa was observed for faults with a dip of 30° developed to the E or W direction. However, after 500 years, the range of CFS change of 2 MPa or more was wider, and it was locally over 4 MPa in the same fault direction as in the previous time period. Even after 10,000 years, a CFS change of more than 1 MPa was still observed in a fault with a slope of approximately 10°. The relatively high fault reactivation region was observed to be biased towards the West and high dip angles over time.

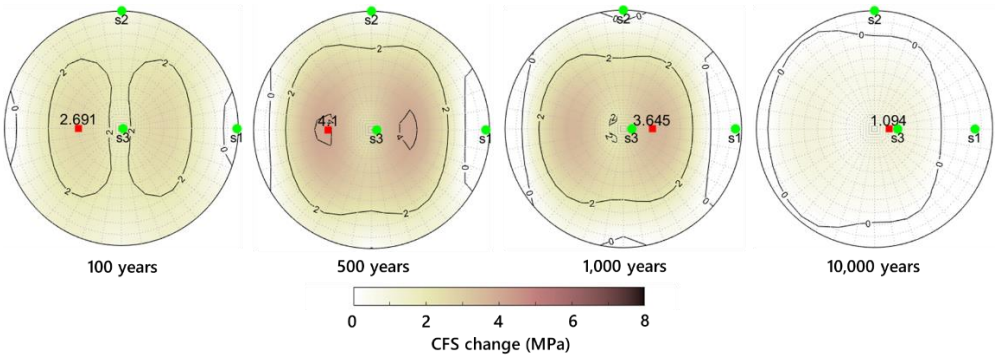

Figure 5.6 Evolution of CFS change with time at a point (1175, 0, -500) in the double-canister disposal system, showing the direction of principal thermal stresses as green colored points and the maximum CFS change as red colored points.

For the double-layered disposal system, the CFS changes over time at point DL-A, which was placed between two layers, and at points DL-B and DL-C, which were 200 m away from the boundary of each layer, were plotted using the stereonets (Figure 5.7). At point DL-A, the largest increase in the CFS was observed near the dip of 30° regardless of the dip direction of the fault, and the increase in the CFS at this point was lower than those of other points, and the area was not relatively wide. As mentioned previously, relatively large CFS changes were observed in points DL-B and DL-C, which are in the vicinity of the boundary at the disposal depth. The fault with a dip of 30° and a dip direction of 90°, which was used as reference in this study, exhibited similar CFS increase at both depths, but the possibility of the fault reactivation at 500 m was higher when all the dip and dip direction of the fault were considered. Additionally, the eastern fault at a depth of 500 m and the western fault at a depth of 700 m are relatively stable.

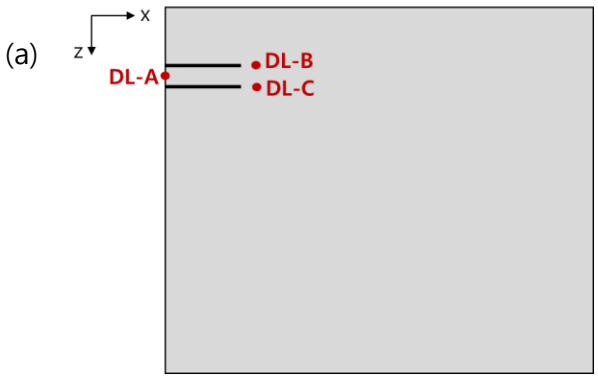

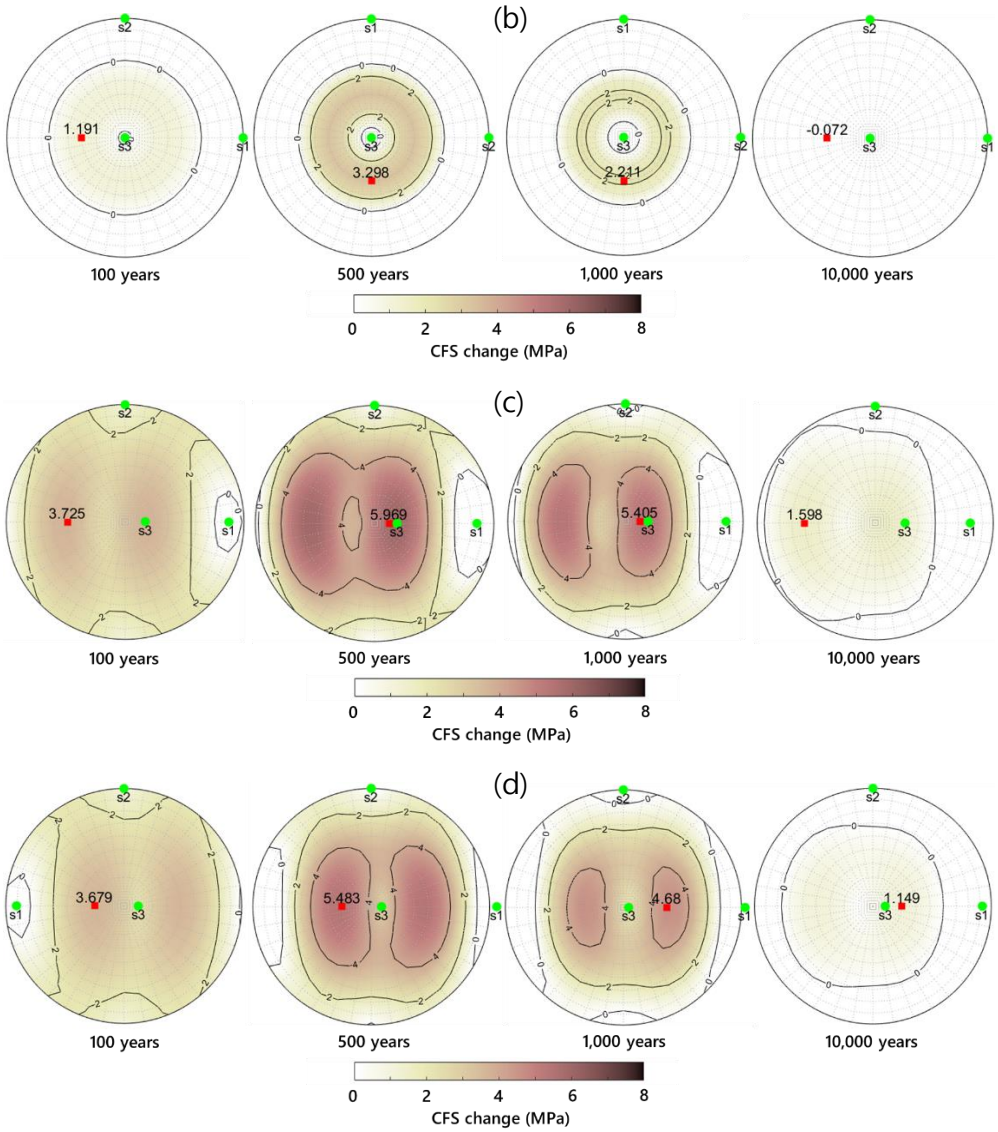

Figure 5.7 Evolution of CFS change with time in the double-layered disposal system, showing the direction of principal thermal stresses as green colored points and the maximum CFS change as red colored points (a) Position of the monitoring points (b) point DL-A (0, 0, -600) (c) point DL-B (950, 0, -500) (d) point DL-C (950, 0, -700)

For the triple-layered disposal system, the CFS change at a distance of 200 m from the boundary of the disposal system at the middle depth and between the layers are plotted on the stereonets (Figure 5.8). Compared to the double-layer disposal system, the increase or decrease in the CFS in the triple-layered disposal system was very low between the layers, such as point TL-B. As shown in Figure 5.8 (b), the CFS increased to a maximum value of approximately 1.5 MPa after 10 years, which was a very early time period. Thereafter, it changed to a negative value, and increased slightly after 500 years, but decreased again and maintained a negative value at all the faults. Considering that the increase in the CFS between the layers in the double-layered disposal system was not remarkably large compared to other points, it seems that the possibility of the stabilization of the faults in the multi-layered disposal system increased with an increase in the number of layers. As shown in Figure 5.8 (c), at a distance of 200 m from the boundary of the disposal system at a depth of 700 m, the possibility of the fault reactivation appears to be high when the fault exhibited a dip direction of approximately 20 to 40° in the NE and NW directions. In addition, the amount of change in the CFS according to the direction of the fault was generally similar to that of the multi-layered disposal system.

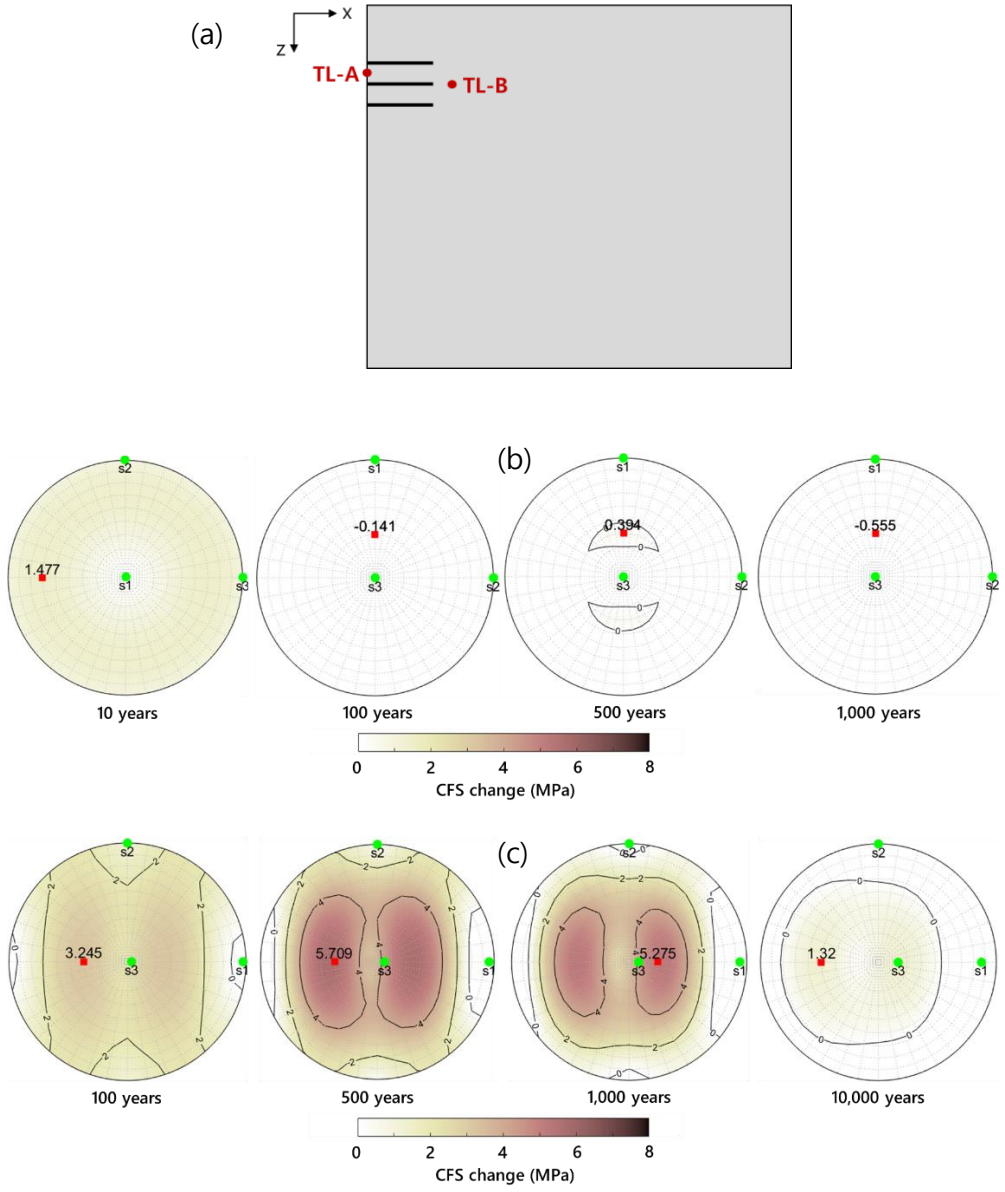

Figure 5.8 Evolution of CFS change with time in the triple-layered disposal system, showing the direction of principal thermal stresses as green colored points and the maximum CFS change as red colored points (a) Position of the monitoring points (b) point TL-A (0, 0, -600) (c) point TL-B (825, 0, -700)

5.3 Effect of the fault property on the CFS change

This section presents the parametric study performed to demonstrate the change in the CFS with a change in the fault property. The friction coefficient, which is largely related to the fault slip, was analyzed by setting its values as 0.4, 0.6, and 1.0. The value of 0.6 is as a reference value used in the previous section. The likelihood of a slip increased with a decrease in the friction coefficient. Figure 5.9 shows the contoured CFS change according to the different friction coefficient value on the xz-plane in the reference disposal system after 1,000 years. The middle image in Figure 5.9 shows the distribution of the CFS change at the reference value. When the friction coefficient was small (i.e., 0.4), the overall area where CFS increased becomes wider. In contrast, when the friction coefficient was large (i.e., 1.0), the CFS increase at the disposal depth also decreased by approximately 2 MPa, and the area where the CFS decreased was further expanded than that of the reference value.

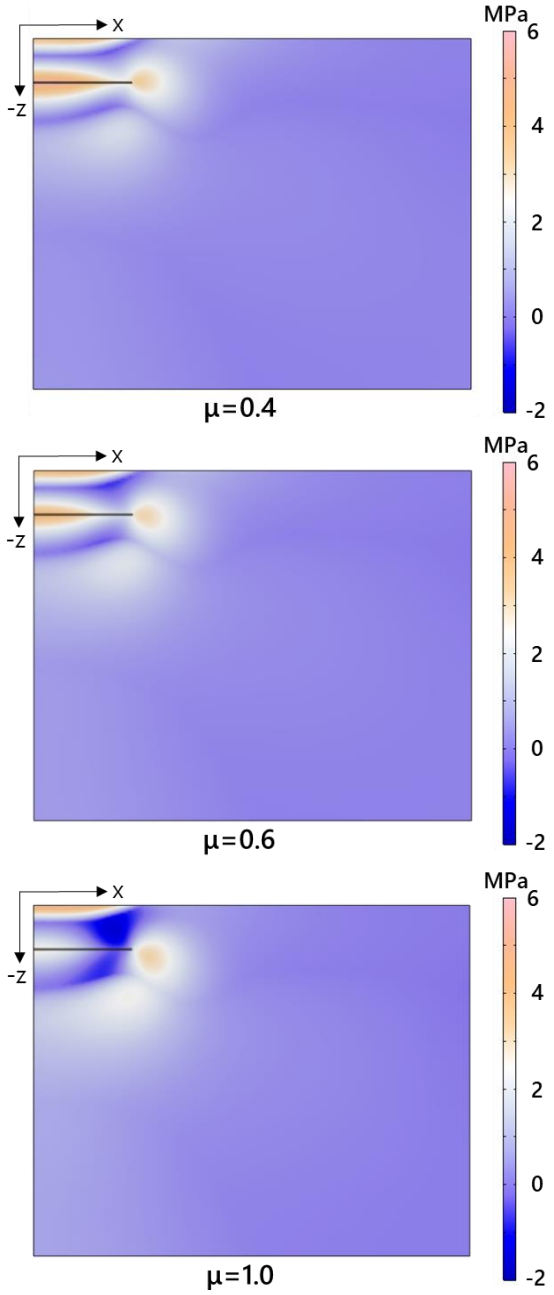

Figure 5.9 Distribution of CFS change on xz-plane according to the different friction coefficient in the reference disposal system after 1,000 years

Moreover, in a location where tensile normal stress occurs, the risk of fault reactivation may increase as the friction coefficient increases. Figure 5.10 (a) shows the change in the CFS with time at point R-B (a distance of 50 m from the boundary of the disposal system), and figure 5.10 (b) shows the change in the CFS at the center of the surface, which is immediately above the disposal system. At point R-B, until 1,000 years, the amount of change in the pore pressure was larger than the normal stress acting on the fault; thus, the CFS change increased with an increase in the friction coefficient. However, after approximately 1,000 years, the increase in the normal stress was larger than the change in the pore pressure, and the CFS change increased with a decrease in the friction coefficient. At the center of the ground surface, a largely horizontal tensile stress was generated. Therefore, the normal tensile stress will be exerted on the designated fault plane, which resulted in the risk of a decrease in the fault reactivation with a decrease in the friction coefficient.

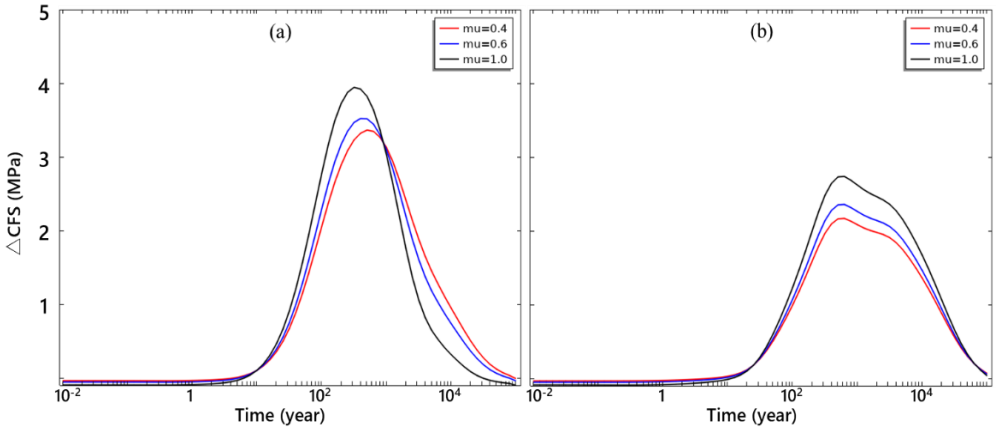

Figure 5.10 CFS change evolution with time at two points in the reference disposal system at (a) a point R-B (1175, 0, -500) (b) a center of the ground surface (0, 0, -500)

If the friction coefficient of the fault surface changed, the weak dip angle at which the fault slip of the fault occurs also changed. Therefore, the mechanism of the effect of the friction coefficient of the fault on the CFS change according to the direction of the fault was analyzed using stereonet. For example, at point R-B, which was previously set when analyzing the CFS change according to the fault direction, the CFS change according to the friction coefficient after 500 years is shown in stereonet (Figure 5.11). When the friction coefficient was small (0.4), the area of the fault with increased CFS was larger, and the area decreased with an increase in the friction coefficient to 1.0. Particularly, the risk of fault reactivation was highest at a dip of 80, 70, and 60° when the friction coefficient was 0.4, 0.6, and 1.0, respectively.

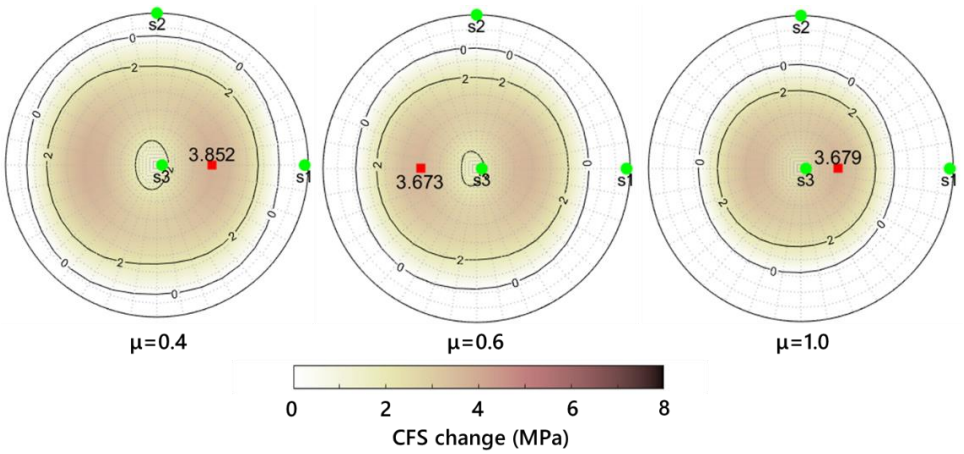

Figure 5.11 Evolution of CFS change after 500 years according to the different friction coefficient at a point R-B

Chapter 6. Discussions

As mentioned in chapter 2, a very small increase in the CFS (approximately 0.01 MPa) can trigger an earthquake when the fault is under a critically stressed state. Thus, the increase in the CFS in this study by several MPa implies that there is a possibility of fault reactivation due to decay heat from HLW around the geological repository. The possibility of fault reactivation varied significantly depending on the direction of thermal stress and the orientation of the fault, and the friction coefficient and the change in pore pressure were observed to significant affect fault reactivation. The evaluation of the CFS to assess the possibility of fault reactivation conducted in this study is conservative. Thus, there are two related discussions that should be considered when assessing the fault reactivation around the disposal system, and they are summarized below.

- Thermal pressurization

  Under impermeable conditions, thermal pressurization induced by frictional heating increases pore pressures (Rice, 2006) and is believed to contribute to slip-weakening behavior during an earthquake (Tanikawa et al., 2014). Particularly, numerous experiments and studies have been conducted on thermal pressurization in clay formation, but there is a lack

of studies on the thermal pressurization of granite. In the hydraulic results of this study, an increase in the pore pressure to up to 3.5 MPa in the middle of the reference disposal system and up to 6 MPa in the middle of the triple-layered disposal system occurred. When the friction coefficient was 0.6, which is the reference value, a 3.5 MPa increase in the pore pressure resulted in a CFS increase of approximately 2 MPa. The average thermal pressurization coefficient in this case was calculated using numerical analysis to be approximately 0.1–0.15 MPa/K. Thermal pressurization is affected by the drained bulk modulus, fluid bulk modulus, porosity, and coefficient of thermal expansion (Tamizdoust and Ghasemi-Fare, 2020). In this study, the numerical models considered the fractured rock as a continuum matrix. This indicates that an increase in pore pressure could be exaggerated because the flow through the fracture was not considered. In addition, in the deep underground, the thermal pressurization effect can be stronger owing to the large confined stress condition. Therefore, based on different assumptions and conditions of the rock mass, experimental verification of the thermal pressurization effect in granite and further studies on its effect on fault reactivation are necessary.

- In situ stress condition

The fault reactivation was analyzed by calculating the change in CFS based on the change in the normal stress, shear stress, and pore pressure on the inclined fault plane due to decay heat. The final risk of fault reactivation in the field may depend on the initial CFS and the initial stress condition. Particularly, if the initial CFS value at the disposal depth is calculated based on the initial stresses presented in Synn et al. (2013), it was calculated to be distributed in stable state between -5 and -1.6 MPa depending on the fault direction. This indicates that even if the CFS change calculated in this study was large, fault reactivation might not occur if it was initially stable. Nevertheless, this study can be useful in that by calculating the amount of the CFS change, it suggested the direction of the fault with a high risk of fault reactivation and the area with the overall risk of fault reactivation around the reference and the alternative disposal systems.

Chapter 7. Conclusions

In this study, to assess the fault reactivation around the geological repository of HLW, 3D coupled THM numerical models of the reference and the alternative disposal systems, including double-canister, double-layered, and triple-layered disposal system, were constructed. Among the reference and the alternative disposal systems, the triple-layered disposal systems exhibited the largest increase in temperature (> 40 ℃) and pore pressure (6 MPa). In addition, the maximum ground heaving (0.43 m), which occurred gradually for a very long time of more than 1,500 years, was observed in the double-layered disposal system. The maximum ground heaving angle and velocity were also the largest in the double-layered disposal system.

With the assumed fault plane with a direction of 90/30, the CFS change in each disposal system was analyzed. At the disposal depth, the maximum CFS change was observed near the boundary of all the disposal system. In addition, with an increase in the time step, the increase in the CFS decreased after the maximum value was attained, but the distance over which the increase was distributed increased to a distance of 3,000 m away. Particularly, the CFS change increased significantly in three areas: at the ground surface above the disposal system, near the boundary of the disposal system, and the center of the disposal system. The generation of the horizontal tensile stress at the

ground surface, vertical tensile stress near the boundary, and horizontal compressive stress at the center of the disposal system contributed to the increase in the possibility of the fault reactivation. The maximum increases in CFS were observed as 4.2, 4.9, 5.3, and 5.6 MPa in the reference, double-canister, double-layered, and triple-layered disposal system.

The analysis of the CFS change according to direction of the fault revealed that the CFS change was significantly affected by the dip regardless of the dip direction in the center of the disposal system. In the vicinity of the boundary of the disposal system, however, the possibility of fault reactivation was high in the dip direction of the principal thermal stress direction. With a change in the location of the monitoring point, the dip and dip direction of the fault with the maximum CFS change also changed. The distance to which the CFS increased significantly above 1 MPa was observed up to approximately 1,000 m from the disposal system. However, after 10,000 years, the CFS change decreased to approximately 1 MPa near the disposal system, but the CFS increase larger than 0.01 MPa was observed up to 3,000 m from the boundary of the disposal system. This indicates that even at a distance of few kilometers from the disposal system, there is a possibility of fault reactivation in the direction of the principal thermal stresses.

Consequently, although the final disposal area can be reduced in the alternative disposal systems up to 44 % of the reference disposal area in the triple-layered disposal system, the thermal stress and possibility of fault

reactivation could be increased. In the alternative disposal systems, the direction of the fault and the distance where the CFS increases would be wider than the reference disposal system. If the in-situ stress condition of the site of the geological repository is sufficiently stable to permit a negligible CFS change, the triple-layered disposal system can be considered a good system to increase the disposal efficiency. However, as the area of possibility of fault reactivation is wider than that of the reference disposal system and the maximum value of ground heaving is high by approximately 10 cm, it is important to investigate these aspects with greater details of site information to secure stability.

Reference

The Atomic Energy Promotion Commission (AEPC), The National Basic Plan for HLW Management, MO- TIE, July 25, 2016 (2016)

COMSOL (1998). Introduction to COMSOL multiphysics extregistered. COMSOL Multiphysics, Burlington, MA, Accessed Feb, 9, 2018.

Ghabezloo, S., & Sulem, J. (2009). Stress dependent thermal pressurization of a fluid-saturated rock. Rock Mechanics and Rock Engineering, 42(1), 1-24.

Ghassemi, A., & Zhang, Q. (2004). A transient fictitious stress boundary element method for porothermoelastic media. Engineering analysis with boundary elements, 28(11), 1363-1373.

Guo, T., Tang, S., Sun, J., Gong, F., Liu, X., Qu, Z., & Zhang, W. 2020. A coupled thermal-hydraulic-mechanical modeling and evaluation of geothermal extraction in the enhanced geothermal system based on analytic hierarchy process and fuzzy comprehensive evaluation. Applied Energy, 258, 113981.

Harris, R. A. (1998). Introduction to special section: Stress triggers, stress shadows, and implications for seismic hazard. Journal of Geophysical Research: Solid Earth, 103(B10), 24347-24358.

Harris, R. A. (2000). Earthquake stress triggers, stress shadows, and seismic hazard. Current science, 1215-1225.

Jaeger, J. C., Cook, N. G., & Zimmerman, R. (2009). Fundamentals of rock mechanics. John Wiley & Sons.

Kim, H.C. and Lee, Y., 2007, Heat flow in the republic of Korea, Journal of Geophysical Research, 112, B05413.

Kwon, S., & Min, K. B. (2021). Fracture transmissivity evolution around the geological repository of nuclear waste caused by the excavation damage zone, thermoshearing and glaciation. International Journal of Rock Mechanics and Mining Sciences, 137, 104554.

Lee, C., Lee, J., Park, S., Kwon, S., Cho, W. J., & Kim, G. Y. (2020a). Numerical analysis of coupled thermo-hydro-mechanical behavior in single-and multi-layer repository concepts for high-level radioactive waste disposal. Tunnelling and Underground Space Technology, 103, 103452.

Lee, J. (2014). Implicit and Explicit Fracture Shear Slip Analysis for Geological Storage of Carbon Dioxide and Nuclear Waste. Seoul National University.

Lee, J., Kim, I., Ju, H., Choi, H., & Cho, D. (2020b). Proposal of an improved concept design for the deep geological disposal system of spent nuclear fuel in Korea. Journal of Nuclear Fuel Cycle and Waste Technology (JNFCWT), 18(spc), 1-19.

Lee, J., Kim, H., Lee, M., Choi, H. J., & Kim, K. (2017). Analyses of the Double-Layered Repository Concepts for Spent Nuclear Fuels. Journal of Nuclear Fuel Cycle and Waste Technology (JNFCWT), 15(2), 151-159.

Lee, J., Cho, D., Choi, H., and Choi, J., (2007), Concept of a Korean reference disposal system for spent fuels, Journal of Nuclear Science and Technology, 44(12), 1565-1573.

Li, P., Chalaturnyk, R. J., & Polikar, M. (2004). Issues with reservoir geomechanical simulations of the SAGD process. Journal of Canadian Petroleum Technology, 43(05).

Mainguy, M., & Longuemare, P. (2002). Coupling fluid flow and rock mechanics: formulations of the partial coupling between reservoir and geomechanical simulators. Oil & Gas Science and Technology, 57(4), 355-367.

McTigue, D. F. (1986). Thermoelastic response of fluid-saturated porous rock. Journal of Geophysical Research: Solid Earth, 91(B9), 9533-9542.

Min, K. B., Lee, J., & Stephansson, O. (2013). Implications of thermally-induced fracture slip and permeability change on the long-term performance of a deep geological repository. International Journal of Rock Mechanics and Mining Sciences, 61, 275-288.

Reasenberg, P. A., & Simpson, R. W. (1992). Response of regional seismicity to the static stress change produced by the Loma Prieta earthquake. Science, 255(5052), 1687-1690.

Rice, J. R. (2006). Heating and weakening of faults during earthquake slip. Journal of Geophysical Research: Solid Earth, 111(B5).

Stein, R. S. (1999). The role of stress transfer in earthquake occurrence. Nature, 402(6762), 605-609.

Synn, J.-H., Park, C., Lee, B.-J. (2013). Regional distribution pattern and geo-historical transition of in-situ stress fields in the Korean Peninsula. Tunn. Undergr. Space 23 (6), 457–469.

Tamizdoust, M. M., & Ghasemi-Fare, O. (2020). A fully coupled thermo-poro-mechanical finite element analysis to predict the thermal pressurization and thermally induced pore fluid flow in soil media. Computers and Geotechnics, 117, 103250.

Tanikawa, W., Tadai, O., & Mukoyoshi, H. (2014). Permeability changes in simulated granite faults during and after frictional sliding. Geofluids, 14(4), 481-494.

Tortike, W. S., & Ali, S. M. (1993). Reservoir simulation integrated with geomechanics. Journal of Canadian Petroleum Technology, 32(05).

Urpi, L., Rinaldi, A. P., Rutqvist, J., & Wiemer, S. (2019). Fault stability perturbation by thermal pressurization and stress transfer around a deep geological repository in a clay formation. Journal of Geophysical Research: Solid Earth, 124(8), 8506-8518

Zoback, M. D., & Gorelick, S. M. (2012). Earthquake triggering and large-scale geologic storage of carbon dioxide. Proceedings of the National Academy of Sciences, 109(26), 10164-10168.

김광일, 이창수, & 김진섭. (2021). 수치해석을 활용한 향상된 한국형 기준 고준위방사성폐기물 처분시스템의 열-수리-역학적 복합거동 성능평가. 터널과 지하공간, 31(4), 221-242.

초 록

고준위방사성폐기물에서 방출되는 붕괴열은 열응력을 발생시키고 이는 처분장 주변의 응력 상태를 교란시킴으로써 단층 재활성화를 유발할 수 있다. 현재, 지진의 발생이 처분시스템에 미치는 영향에 대해서는 근계 영역에 대하여 처분용기의 안전성 중심으로 연구가 진행되어 왔으나, 심지층 처분장 주변의 단층 재활성화 가능성에 대해서는 아직 주목받지 못하고 있는 실정이다.

본 연구에서는 한국형 기준 처분시스템 뿐 아니라 처분 면적을 감소하기 위해 대안 처분시스템으로 제안되었던 다층 처분시스템 및 다적층 처분시스템 주위 암반에서의 열-수리-역학적 복합거동을 분석하기 위한 3 차원 원계 수치 모델을 구축하였다. 열-수리-역학적 복합거동의 결과로 처분시스템의 중심부에서는 수평 압축 응력이 발생하고, 처분시스템의 직상부에서는 수평 인장 응력이 크게 발생하였다. 고준위 방사성폐기물로 인한 암반의 열팽창은 지표면 융기를 야기하는데, 다층 처분시스템에서의 최대 지표면 융기가 기준 처분시스템보다 10 cm 크게 발생하였으며, 지표면 융기의 각도와 연간 융기 속도 역시 복층 처분시스템에서 가장 크게 발생하는 것으로 확인되었다.

수치해석 결과를 바탕으로 90/30 방향의 단층에서의 쿨롱파괴응력 변화량을 평가하여 처분시스템 주변에서의 단층 재활성화를 분석하였다. 그 결과 쿨롱파괴응력은 처분시스템의 중심부, 처분시스템의 직상부, 그리고 처분시스템의 경계 근처에서 크게 증가하였다. 또한, 다른 모델에 비해 삼층 처분시스템의 중간 처분 깊이인 700 m 경계 부근에서 가장

큰 쿨롱파괴응력 증가량이 관측되었다. 뿐만 아니라 모든 단층의 경사 및 경사방향을 고려하여 단층 재활성화 위험도를 평가하고 이를 평사도법으로 도시한 결과, 처분시스템의 중심에서는 단층의 경사에 따라 쿨롱파괴응력 변화량이 결정되었다. 이와 달리 처분시스템의 경계 부근에서는 주된 열응력 발생 방향에 따라서 단층의 경사와 경사방향에 의해 쿨롱파괴응력 변화량이 결정되었으며, 상대적으로 완만한 경사에서 단층 재활성화 위험도가 증가한다. 약 10,000 년 정도로 오랜 시간이 지나더라도 처분 깊이에서는 처분시스템 경계에서 약 3 km 떨어진 지점까지 쿨롱파괴응력 증가할 수 있음이 확인되었다.

결론적으로, 대안 처분시스템의 경우, 처분 단면적 자체는 기준 처분시스템에 비해 상당히 감소시킬 수 있으나 단층 재활성화 위험도의 가능성과 그 범위 그리고 지표면 융기는 더 증가한다. 이러한 단층 재활성화 위험도는 단층의 초기 응력 상태와 마찰 계수 등의 성질에 따라 상이하므로, 대안 처분시스템을 적용하기 위해서는 이에 대한 정확한 정보와 안정성을 확보하는 것이 중요하다.

주요어: 고준위 방사성폐기물 심지층 처분장, 대안 처분시스템, 열-수리-역학적 모델링, 쿨롱파괴응력, 단층 재활성화